AD-A094 348 NAVAL RESEARCH LAB WASHINGTON DC F/G 21/2
A COMPUTATIONAL STUDY OF THE CHEMICAL KINETICS OF HYDROGEN COMB--ETC(U)
JAN 81 T L BURKS, E S ORAN
UNCLASSIFIED NRL-MR-4446 NL

END
DATE FILMED
3-81
DTIC

(14) NRL-MR-4446

SECURITY CLASSIFICATION OF THIS PAGE (When Data Entered)

(9) REPORT DOCUMENTATION PAGE

READ INSTRUCTIONS BEFORE COMPLETING FORM

1. REPORT NUMBER: NRL Memorandum Report 4446	2. GOVT ACCESSION NO.: AD A094 348
3. RECIPIENT'S CATALOG NUMBER:	
4. TITLE (and Subtitle): (6) A COMPUTATIONAL STUDY OF THE CHEMICAL KINETICS OF HYDROGEN COMBUSTION	5. TYPE OF REPORT & PERIOD COVERED: Interim report on continuing NRL problem
	6. PERFORMING ORG. REPORT NUMBER:
7. AUTHOR(s): (10) T. L. Burks and E. S. Oran	8. CONTRACT OR GRANT NUMBER(s):
9. PERFORMING ORGANIZATION NAME AND ADDRESS: Naval Research Laboratory, Washington, D.C.	10. PROGRAM ELEMENT, PROJECT, TASK AREA & WORK UNIT NUMBERS: NRL-44-0572-0-1, Pro. El. No. 61153N, Pro. No. 0240241
11. CONTROLLING OFFICE NAME AND ADDRESS: NASA, Washington, D.C.	12. REPORT DATE: (11) 28 Jan. 1981
	13. NUMBER OF PAGES: 58
14. MONITORING AGENCY NAME & ADDRESS (if different from Controlling Office): (12) 59	15. SECURITY CLASS. (of this report): UNCLASSIFIED
	15a. DECLASSIFICATION/DOWNGRADING SCHEDULE:

16. DISTRIBUTION STATEMENT (of this Report)

Approved for public release; distribution unlimited

17. DISTRIBUTION STATEMENT (of the abstract entered in Block 20, if different from Report)

18. SUPPLEMENTARY NOTES

19. KEY WORDS (Continue on reverse side if necessary and identify by block number)

Hydrogen
Combustion
Chemical Kinetics
Reaction Kinetics

20. ABSTRACT (Continue on reverse side if necessary and identify by block number)

A set of elementary reactions and their corresponding rate coefficients has been assembled to describe the homogeneous H_2-O_2 reaction system over the temperature range 300-3000°K. The reaction mechanism was drawn together assuming that H_2-O_2 reactive mixtures could be adequately described in terms of self-consistent, thermal distributions of electronically neutral, ground-state reactants, intermediates and products. The resulting time-dependent ordinary differential equations describing the system were integrated assuming various initial pressures, temperatures and initial concentrations of reactants and diluents. The computed results have been compared with experimentally observed induction times, second explosion limits, the rate

(Continued)

251950

20. ABSTRACT (Continued)

of reaction above the second explosion limit and the temporal behavior of reaction species. The good agreement between the computational and experimental results attests to the accuracy of the assembled mechanism in its description of the homogeneous reaction system and supports the validity of the set of associated rate coefficients for the elementary reactions of the mechanism over a broad range of reaction conditions.

CONTENTS

A COMPUTATIONAL STUDY OF THE CHEMICAL KINETICS OF HYDROGEN COMBUSTION

I. INTRODUCTION

A major difficulty in the study of reactive flows is the investigation of the influence of various contributing processes in a system's behavior. Because of this, it is often desirable to examine the component processes separately before attempting to understand their interaction. In combustion systems, for example, it is important to investigate the chemical and gasdynamic processes individually before considering the fully-coupled, nonlinear system. However, the strong coupling between these processes sometimes poses an added problem to their separate and independent study.

In addition to these problems, there are other difficulties that are associated more explicitly with the study of the individual processes. One important problem that arises in the study of the chemistry of combustion systems is the problem of accurately determining the reaction mechanism that describes the system over the range of temperatures, pressures and stoichiometries encountered during combustion. Such a reaction mechanism is usually composed of a set of elementary or primary reactions that involve a number of intermediate species that are produced by initial reactants in their conversion to products. However, even in the simplest chemical kinetic schemes, it is often difficult or nearly impossible to determine all of the elementary reactions, their rates and intermediate species. Experiments can determine the products of combustion and can sometimes detect significant metastable intermediates and define their related reaction cross sections, but inference and supposition are always involved in the assignment of a reaction mechanism.

Manuscript submitted December 2, 1980.

Our efforts in modeling combustion in hydrogen-containing gas mixtures have led us to consider the accuracy with which a proposed $H_2 - O_2$ elementary reaction set describes the chemistry of this system. These considerations are important because hydrogen itself is an important fuel and because its oxidation mechanism plays a fundamental role in the combustion of hydrocarbons. An accurate description of hydrogen combustion is also useful because it will help in the evaluation of the likelihood of deflagration and explosion hazards in industrial facilities such as nuclear reactors. Therefore, the purpose of this paper is to: 1) present a homogeneous, gas-phase reaction mechanism descriptive of the $H_2 - O_2$ combustion system, 2) describe the computational kinetic work that we have done to test the accuracy of the mechanism, and 3) summarize our conclusions regarding the general applicability of this mechanism.

In the work presented here, we have assumed that the individual states of the reacting molecules are equilibrated and that local thermodynamic equilibrium exists. This simplifies the problem and allows us to use the principle of thermodynamic consistency between forward and reverse reactions to compute poorly known reaction rates via the equation:

$$K_{eq} = k_{forward} / k_{reverse}. \tag{1}$$

Here K_{eq} is the thermodynamic equilibrium constant and $k_{forward}$ and $k_{reverse}$ are the reaction rate coefficients for the associated forward and reverse reactions.

In order to test the proposed reaction mechanism, a series of detailed chemical kinetic calculations have been performed. The computational code, referred to as *CHEMOD*, has been described in detail by Flanigan and Young [1]. Briefly, the code consists of three principal parts: 1) an I/O and logical control program, 2) a syntactical reaction transcriptor (SRT) and differential function generator, and 3) a vectorized version of the asymptotic integration method developed by Young [2]. The SRT was developed by Young explicitly for the CHEMOD code. The code computes total molar concentration, total mass density, total pressure, internal energy, and individual species concentrations as a function of time under isothermal or adiabatic constant-volume, ideal-gas reaction conditions.

The results obtained from these calculations have been compared with available measurements of reaction induction times, second explosion limits, the temporal behavior of reaction species and reaction equilibrium parameters. These comparisons have been critically evaluated with regard to the experimental conditions of the measurements. Specifically, contributions by gasdynamic effects have been noted.

II. THE $H_2 - O_2$ REACTION MECHANISM

Ever since the early work of Hinshelwood, Sagulin and Semenov [3-7], the $H_2 - O_2$ reaction system has been the subject of continuous and intensive research [8-13]. In this section, we summarize some of the important features of this system in order to provide a background for the material that follows. In addition, we discuss some of the details pertinent to the mechanism that we have used to describe the $H_2 - O_2$ reaction system.

The gas-phase reaction between H_2 and O_2 is a complex reaction system composed of a relatively large number of elementary reactions. The system consists of a chain reaction sequence that branches between the atomic and free radical chain carriers H, O, HO and HO_2. At low temperatures, HO_2 is only moderately reactive and is important in chain termination. At temperatures above $\sim 1500°K$, HO_2 is more reactive and becomes an effective chain carrier.

A principal feature of the $H_2 - O_2$ reaction system is its demonstration of explosion limits that vary as a function of pressure and temperature. Information about these limits was initially deduced from observations made in static cell experiments [14-22]. These studies showed that cell dimensions and wall surface materials are important factors and led to the conclusion that heterogeneous reactions make important contributions in the $H_2 - O_2$ system. This is especially true at the first explosion limit. The second explosion limit is also affected, but to a much lesser extent.

Figure 1 shows the explosion limit diagram as a function of pressure and temperature for a stoichiometric mixture of H_2 and O_2. This figure can be qualitatively understood in terms of the relationship between chain branching and chain termination first pointed out by Semenov [9] and Hinshelwood [8]. They have shown that whenever the rate of chain branching exceeds the rate of chain termination, fast combustion occurs. Inversely, whenever the rate of chain termination exceeds the rate of chain branching, H_2 and O_2 react slowly.

Thus, at initial pressures below the first explosion limit (where the mean free path of the chain carriers is comparable to reaction vessel dimensions), chain termination by heterogeneous wall reactions predominates and a slow reaction is observed. As the pressure of the reaction mixture is increased (and the mean free path of the chain carriers is decreased), the rates of the bimolecular chain branching and propagation reactions are increased relative to the heterogeneous chain termination reactions. Finally, chain branching exceeds chain termination at the first explosion limit and the overall rate of the reaction increases exponentially.

Between the first and second explosion limits, in the region of the explosion peninsula, the gas mixture explosively ignites at all pressures. At the second explosion limit, chain termination by termolecular reactions becomes important. As the pressure of the reaction mixture is increased to just above the second explosion limit, the rate of termolecular chain termination overbalances the rate of chain branching and a slow reaction between H_2 and O_2 again predominates. The overall rate of reaction between H_2 and O_2 then decreases to a minimum and then begins to slowly increase as the pressure is raised above the second explosion limit. The overall reaction rate continues to increase with increasing pressure until the rate of thermochemical heat release exceeds the rate of heat removed. In this region, the reactions become self-accelerating, or autocatalytic, and the third explosion limit becomes defined. At pressures above the third explosion limit, it is thought that all pressures ignite to explosion.

The H_2-O_2 reaction mechanism tested in this work includes all likely homogeneous, gas-phase reactions among all feasible neutral, electronic ground state species. Reactions were not included that involved mechanistically difficult atomic rearrangements equivalent to the operation of two or more other elementary reactions. Where available data showed that a reaction was not well-known, this reaction was omitted. The reaction mechanism incorporates termolecular reactions presuming that the major third body constituent of these reactions is a heavy inert species such as argon. In Table 1, we present the mechanism as a series of forward and reverse elementary reactions and rate constants.

Reaction rate constants were chosen from a survey of available data and are expressed in the modified-Arrhenius form:

$$k(T) = AT^B \exp(C/T) \tag{2}$$

where $k(T)$ is the temperature-dependent reaction rate constant, T is temperature (°K) and A, B and C are constants. For those reactions for which rate constant information was either sparse or not known at all, an individual rate constant was computed using Equation (1).

Concentration-based equilibrium constants, K_{eq}^c, were cast into the same modified-Arrhenius form as the reaction rate constants. A third-order matrix expression was constructed by selecting thermodynamic equilibrium constant data at three points that spanned the 300-3000°K temperature range for the following equation:

$$\ln K_{eq,i}^c = \ln A_{eq} + B_{eq} \ln T_i - C_{eq}/T_i \tag{3}$$

where $K_{eq,i}^c$ and T_i are the equilibrium constant and temperature of the i th point and A_{eq}, B_{eq} and C_{eq} are constants. The thermodynamic data was taken from the JANAF Tables [23] and from Engleman's compilation of kinetic data [24]. Solution of the matrix relation for the three constants—A_{eq}, B_{eq} and C_{eq}—for each forward and reverse reaction pair then provided for the temperature-dependent description of the equilibrium constants as shown in Table 2.

Forward and reverse reaction rate constants were checked for thermodynamic consistency over the 300-3000°K temperature range by comparison of temperature plots of reaction rate constants obtained by experiment and by use of Equation (1). When a rate constant was either poorly known experimentally or was not consistent with its reverse rate and equilibrium constant, the computed rate constant was used in lieu of the experimental rate constant. Since there are frequently more problems and larger errors associated with the measurement of rate constants at elevated temperatures, most of the computed rate constants are among the endoergic reactions listed as reverse reactions in Table 1. Three examples of reactions that were found to be thermodynamically inconsistent are shown in Figures 2-4.

The use of the thermodynamic equilibrium relationship to compute unknown rate constants is based on the assumption that the elementary reactions of the H_2-O_2 combustion system involve reactants, intermediates and products that can be described by Boltzmann thermal energy distributions. This condition is generally correct in the slow reaction zones of concentrated gas mixtures and even in the explosively reactive zones of highly diluted gas mixtures. The assumption is supported by the work of Asaba et al. [25] and Belles and Lauver [26] who have shown that vibrational equilibration of O_2 in shock-initiated combustions only affects the H_2-O_2 reaction kinetics by a very small amount. Thus, since it appears that large shock-induced disturbances are satisfactorily equilibrated within the induction time of the reactive gas mixture, we presume that more uniform energy perturbations due to combustion (exclusive of explosion) are efficiently relaxed so that equilibrium kinetics can be assumed.

The modified-Arrhenius form of reaction rate constants that is commonly used has been obtained by empirical data fitting. Although transition state (or activated complex) theory [27-29] and collision theory [30-32] predict non-Arrhenius temperature behavior, neither theory provides an explicit, analytical temperature dependence for the rate constant, $k(T)$.

Justification for the use of the modified-Arrhenius rate constants has been provided by a number of workers [27-36]. Zellner [28] has recently shown that the additional temperature dependences can be understood in terms of large variations in state-specific rate constants, k_i. In other words, the

vibronic states of an electronic ground state reactant can react at different rates. Birely and Lyman [37] have reviewed the state-specific (or microscopic) rate constant literature and have found a large body of experimental evidence that points to a trend towards greater reactivity with increasing internal excitation. As an example, Spencer et al. [38] have considered the reaction

$$HO + H_2 \rightarrow H_2O + H \tag{4}$$

and found that vibrational excitation of HO did not substantially affect the overall rate of reaction. However, Zellner et al. [28] observed that H_2 vibrational excitation provided significant state-specific rate constant enhancement. Specifically, they found

$$k_{HO+H_2(v=1)}/k_{HO+H_2(v=0)} \cong 1.5 \times 10^2. \tag{5}$$

Thus, the additional temperature dependence of the macroscopic rate constant for the HO + H_2 reaction, as shown by the concave-upward curvature of the log $k(T)$ versus 1000/T plot in Figure 5, results *from the variation in reactivity of* one of its reactants, $H_2(v)$, as a function of temperature. This does not require nonequilibrium thermal distributions of energy among reactants, but is compatible with a Boltzmann distribution of reactants over accessible vibronic states.

Of exceptional value in the assembly of the H_2-O_2 reaction mechanism has been the compilation of Baulch et al. [39] at Leeds University. Although we conducted a literature search to update the rate constants in this compilation, very little difference was found in the rate constant reports following their publication date of 1971.

III. INDUCTION TIME CALCULATIONS

A. Background

Reaction induction times, also called ignition delay times, have become important parameters measured in chemical kinetic studies. Although a number of workers had previously studied induction times in the H_2-O_2 system [40-41], Schott and Kinsey were one of the first to use these measurements

to examine $H_2 - O_2$ reaction kinetics [42]. In these experiments, they showed the inverse dependence of induction time on $[O_2]$ and were able to calculate a rate coefficient for the important chain branching reaction, $H + O_2 \rightarrow HO + O$. Following these initial investigations, a large amount of work was devoted to the elucidation of the details of the $H_2 - O_2$ mechanism using induction time measurements. This information has been reviewed by Schott and Getzinger [43].

The induction time of a reaction is defined to be the length of elapsed time between the time of reaction initiation and the time when reaction is first observed. Ambiguity arises when this definition is applied to: 1) a system in which reaction initiation is not instantaneous and 2) a system where reaction observation depends upon the sensitivity and specificity of the observing apparatus.

Ambiguity concerning reaction initiation is usually resolved by limiting the determination of reaction induction times to experimental apparatus in which the rise time of a temperature jump or of a reactive species concentration is of the order of a few microseconds or less. Reaction perturbations with rise times this short have generally been found to satisfy effectively the constraint of instantaneous reaction initiation.

The end of the induction period is often obvious since, even for large variations in reaction conditions, it is usually associated with an exponential growth of intermediate species concentrations. This situation is generally accompanied by similar increases in pressure and temperature. Thus, variations in sensitivity and specificity between apparatus conforming to the instantaneous reaction initiation criterion should only result in small systematic discrepancies in data.

Because of the above considerations, shock-tube experiments represent one of the principal methods used to measure induction times. In addition to approximating instantaneous reaction initiation, these experiments usually provide at least two other desirable features: 1) isothermal and 2) homogeneous reaction conditions.

A near isothermal reaction condition is achieved when thermochemical effects are mitigated by the dilution of reactive mixtures. Diluents commonly used are inert gases such as argon and helium. There is, however, another factor peculiar to shock-tubes that causes deviations from the ideal isothermal reaction condition. This has been discussed by Belles and Brabbs [44] and Mirels [45] who have shown that boundary layer growth in the flowing gases behind incident shocks can increase gas temperature, density and particle residence time. In those shock-tube experiments that do not account for this effect, incorrect temperature estimates can result. Studies that are most likely affected involve reactions having high activation energies. Consequently, it is generally held that reaction rate coefficients obtained by shock-tube measurements prior to $\sim$1970 (when it became common practice to make boundary layer corrections) should be suspected of high apparent values. Similarly, induction time measurements made in shock-tube experiments not correcting for boundary layer effects should be suspected of being underestimated.

Another advantage of shock-tube experiments is that they permit data to be collected in time periods that are short in comparison to gas diffusion rates. This eliminates the possibility of heterogeneous wall reactions. Since the elementary reaction mechanism contained in Table I consists solely of homogeneous reactions, shock-tube measurements should provide excellent data for testing numerical calculations using this reaction set.

Studies of the variation of H_2-O_2 reaction induction time as a function of pressure, temperature and reactant composition have identified two principal regions of ignition. Schott and Kinsey [42] observed that above $\sim$1100°K and below $\sim$2 atm (the high-temperature, low-pressure region, which we shall designate "HTLP") their induction time measurements could be related by:

$$\log_{10}\{[O_2]_i \tau_i\} = A + B/T \tag{6}$$

where $[O_2]_i$ is the initial O_2 concentration, τ_i is the induction time, A and B are constants and T is the temperature. They derived this expression from a partial steady state analysis of the following mechanism:

$$H_2, O_2 + M \rightarrow H, O, HO + M$$
$$H + O_2 \rightarrow HO + O$$
$$O + H_2 \rightarrow HO + H$$
$$HO + H_2 \rightarrow H_2O + H$$
$$H + O_2 + M \rightarrow HO_2 + M$$

Miyama and Takeyama [46] carried out similar experiments to those of Schott and Kinsey and were also able to identify an inverse dependence of induction time on $[O_2]_i$. However, when Miyama and Takeyama extended their induction time experiments to temperatures below $\sim$1100°K and pressures above $\sim$2 atm (the low-temperature, high-pressure region, which we shall designate "LTHP"), they observed two consecutive temporal jumps in HO concentration. The first HO concentration rise was not accompanied by a pressure increase, whereas the second HO concentration was associated with a simultaneous jump in pressure. Their attempts to understand their pressure-jump data did not show a correlation of induction times with $[O_2]_i$, but did show a correlation with $[H_2]_i$. Similar results were obtained by Strehlow and Cohen [47], Fujimoto [48] and Skinner and Ringrose [49]. In addition to these observations, Soloukin and coworkers [50] and Meyer and Oppenheim [51] have reported that their schlieren experiments have shown two distinct types of ignition. A sharp, or single source, fast ignition was observed in the HTLP region and a mild, or multiple source, slow ignition was observed in the LTHP region.

A qualitative understanding of the characteristics that differentiate the two regions of H_2-O_2 ignition can be obtained by considering the extended second explosion limit shown in Figure 6. Brokaw [52] has derived an analytic solution of a simplified reaction mechanism that simulates the different behavior found in the "sharp" and "mild" ignition region. In addition, Wakefield, Ripley and Gardiner [53] have demonstrated the origins of some of those differences by comparing analytic and numeric solutions of a more detailed reaction mechanism. In brief, the results of these studies have shown that the two regions of ignition are separated by the extended second explosion limit, at which the rate of chain branching is balanced by the rate of chain termination. To the left of the extended second limit, in the LTHP region, the HO_2 concentration becomes significant and its bimolecular reactions become

important in mild ignition. To the right of the extended second limit, in the HTLP region, chain branching reactions among H, O and HO dominate and lead to sharp ignition.

B. Results

The information discussed above indicates that homogeneous reactions predominate in both the LTHP and HTLP regions of ignition in H_2-O_2 gas mixtures. Thus, we have calculated H_2-O_2 reaction induction times for both regions using the mechanism given in Table I. For the LTHP region, we have computed a set of induction times for initial conditions descriptive of the work by Skinner and Ringrose [49]. These are shown in Figure 7. For the HTLP region, we have calculated a series of induction times using the reaction conditions of White [54]. These data are presented in Table 3. The agreement between the calculated and experimental induction times found in both the HTLP and LTHP regions of H_2-O_2 ignition supports the mechanism of Table 1 in its description of the initial phases of reaction.

As a means of investigating the functional behavior of induction time in the H_2-O_2 system, we have performed a number of adiabatic and isothermal calculations while varying initial temperature, pressure and extent of N_2 dilution. Under the conditions of these calculations, N_2 does not participate as a reactant but only as an inert diluent. We show the adiabatic temperature versus reaction time curves that were generated for a stoichiometric H_2-air mixture in Figures 8-11. In these curves, the initial temperature was varied from 900 to 2000°K in 100°K increments for each of the initial pressures 0.05, 0.5, 5 and 50 atm. The times at which the H atom and HO radical intermediates experience their concentration maxima appear to coincide and are indicated by arrows on each curve. It is noted that these times also correspond to the first temperature increases and exponentially increase with decreasing initial temperature. It is also seen that the curves generated in the HTLP regions show a distinctly different form than the curves generated in the LTHP regions. These observations seem to agree with the different ignition patterns reported for these two regions.

In Figures 12-14, we show the induction time dependence on initial temperature and pressure as a function of dilution of a stoichiometric H_2-O_2 mixture. The change in ignition pattern, as demonstrated by induction time, between the LTHP and HTLP regions is observed as a shift toward sharper, exponential increases in induction time with decreasing initial temperature and increasing initial pressure. The dilution effect appears to uniformly increase induction time for the stoichiometric, reactive mixtures and does not significantly change the form of the induction time dependence on initial temperature and pressure. These observations are in agreement with those of Meyer and Oppenheim [51].

The change in behavior of induction time and, thus, ignition may possibly be better demonstrated in Figure 15. In this figure, induction time is plotted as a function of initial pressure for each of three isothermal calculations. Initial temperature conditions were 1000, 1100, and 1500°K. It can be seen that the pressure dependence of induction time clearly makes a shift below 1100°K and above $\sim$2 atm. Mild ignition affected by hydrodynamic interactions with chemistry can be easily imagined in a situation where induction times are relatively long.

IV. SECOND EXPLOSION LIMIT CALCULATIONS

A. Background

The line showing the division between explosive and nonexplosive regions (fast and slow reaction) for a stoichiometric H_2-O_2 mixture contained in a KCl-coated reaction vessel has been shown in Figure 1. The line makes its excursion between $\sim$650-850°K and between $\sim$1-5000 torr and is divided into three segments designated as the first, second and third explosion limits.

As mentioned previously, the three explosion limits have been investigated in static flow experiments that have demonstrated how important the dimensions and materials of the reaction vessels are in determining points of explosion. These observations firmly established the significance of gasdynamic processes in these experiments. They have also shown that the first and second explosion limits depend upon the chain branching chemistry of the H_2-O_2 system [22]. However, there is still

some question concerning the mechanism of the third explosion limit; i.e., whether it is controlled by thermal or chain branching processes [55].

In order to describe the influence of chain reactions at the first and second explosion limits, it has become common practice to consider the concentration of a typical chain carrier [43]:

$$d[C]/dt = I + B[C] - T[C] = I + N[C] \tag{7}$$

where $[C]$ represents chain carrier concentration, I is the initiation rate, B is the rate of chain branching and T is the chain termination rate. The N of Equation (7) is the net sum of the rates of chain branching and chain termination and is an important parameter used in describing the concentration of a chain carrier in the early stages of reaction.

Assuming initial reaction rate conditions, where I, B and T are well-defined and $[C]$ is negligible, Equation (7) may be integrated to give

$$[C] = (I/N)\,[\exp(Nt) - 1]. \tag{8}$$

Two limits of this equation describe the chemistry on opposite sides (slow versus fast reaction) of an explosion limit controlled by chain reaction chemical kinetics. In the first case, where chain termination dominates chain branching (i.e., $T > B$), N is negative and $[C]$ is forced to approach a concentration approximated by (I/N). In the second case, where chain branching overshadows chain termination (i.e., $B > T$), N is positive and $[C]$ exponentially increases with time. In this latter situation, a large amount of heat is released in a short time interval and the total complex of elementary reactions is accelerated to fast reaction (explosion) by thermal feedback or autocatalysis.

The $H_2 - O_2$ mechanism responsible for this behavior may be summarized in terms of its most important reactions. The three elementary reactions of major significance to chain branching in the vicinity of the first and second explosion limits are [42]:

$$H + O_2 \rightarrow HO + O \tag{9}$$

$$O + H_2 \rightarrow HO + H \tag{10}$$

$$HO + H_2 \rightarrow H + H_2O \tag{11}$$

Similarly, chain initiation involves the four-center reaction [56]:

$$H_2 + O_2 \rightarrow 2HO \tag{12}$$

although a number of alternate initiation reactions may play an important role. Where the reactivity of $H >> HO_2$, chain termination occurs principally by the reaction [13]:

$$H + O_2 + M \rightarrow HO_2 + M. \tag{13}$$

In addition, two other termolecular reactions have been shown to be important chain termination reactions [57]:

$$H + HO + M \rightarrow H_2O + M \tag{14}$$

$$H + H + M \rightarrow H_2 + M \tag{15}$$

Although these elementary reactions do not constitute a complete reaction mechanism, they are primarily responsible for many of the features of the first and second explosion limits.

B. Results

Because the second explosion limit is largely determined by the homogeneous chemical kinetics of the $H_2 - O_2$ system, we have tested our mechanism by performing a number of calculations of parameters associated with this limit. Although several other numerical studies, using either abbreviated reaction mechanisms or varying individual reaction rate coefficients, have examined the second explosion limit [55,58,59], we have based our evaluations on straightforward computations involving a complete reaction set. We have not varied the rate coefficients to achieve better fits to data. In these calculations, it was not our purpose to fit a parameter but rather to compare computed and experimental results and to try to understand the significance of any agreement or disagreement.

As a first step, we have made a series of calculations describing a 0.5 atm, H_2:O_2/2:1 reaction mixture at 10°K intervals from 808 to 848°K. The behavior of intermediate species concentrations was followed temporally and was recorded as a function of initial temperature.

As shown in Figures 12-14, we found that reaction induction time increases exponentially with decreasing initial temperature. This behavior is also observed in the temporal plots of the hydroxyl radical concentration presented in Figure 16. The pattern continues up to a temperature between 818 and 828°K, where further reduction of initial temperature results only in linear increases in induction time. At about the same temperature, a part of the exponential growth in HO concentration appears to vanish. This transition occurs within 10°K and appears to be linked to the loss of ignition at the second explosion limit. In addition, we believe that this latter feature may also be tied to the experimental observation of spikes and overshoots of intermediate species concentrations noted in shock-tube experiments conducted close to the second explosion limit [43].

Using the above changes in induction time and hydroxyl radical behavior to define the crossing of the second explosion limit, we have computed a set of points in the temperature-pressure plane that corresponds to the second explosion limit of a stoichiometric H_2-O_2 gas mixture. These results are presented in Figure 17 where they are compared to the experimental work of Lewis and von Elbe [11]. We note that the calculated values show a second explosion limit uniformly lower in temperature than that which was observed in a 7.4 cm diameter, KCl-coated reaction bulb. This discrepancy can be attributed to the fact that we have modeled homogeneous chemistry in a situation where heterogeneous chemistry also plays a part. The displacement of our calculated data towards lower temperatures is consistent with the idea that the absence of heterogeneous termination reactions in our mechanism would require less thermal energy supplied to branching reactions to overbalance chain termination.

By examining the production and loss terms for each chemical species, we have observed that the major reaction channel for consumption of HO changes as the initial reaction temperature is reduced below the second explosion limit. Specifically, the chain branching reaction, $H + O_2 \rightarrow HO + O$ (Equation 9), is replaced by the chain termination reaction, $H + O_2 + M \rightarrow HO_2 + M$ (Equation 13). This observation appears to coincide with the disappearance of the second [HO] exponential increase shown in Figure 16. On the explosive side of the second explosion limit and at the point of ignition,

reaction (13) becomes an insignificant channel for production of HO_2 and reaction (9) becomes a major channel for production of HO. On the nonexplosive side of the second explosion limit, reaction (13) remains the primary channel of formation of HO_2, with an increase in HO_2 concentration followed by enhanced reaction rates for HO_2 and H_2O_2.

Defining the initial reaction rate to be proportional to the rate of formation of H_2O, we have computed this parameter above the second explosion limit. Figure 18 presents the results of a calculaltion of $d[H_2O]/dt$ as a function of pressure along a 760°K isotherm for a stoichiometric H_2-O_2 gas mixture. The behavior of the calculated initial reaction rate above the second explosion limit closely resembles that experimentally determined by Lewis and von Elbe [60]. As the pressure of the reactive gas mixture is raised above the second explosion limit, the initial reaction rate falls rapidly from extremely large values to a minimum and then begins to gradually climb as pressure is increased.

V. *THE TEMPORAL BEHAVIOR OF REACTION SPECIES*

A. Background

Since a good deal is known about the individual elementary reactions of the H_2-O_2 system (specifically, their rate coefficients as a function of temperature), it is possible to test the complete reaction mechanism by comparing computed and observed temporal profiles of reaction species concentrations. In the shock-tube, temporal profiles of species concentrations have been determined typically as a function of the stage of H_2 combustion. Moreover, these experimental profiles have not been published in simple, time-based plots of species concentrations, but are commonly used to derive other quantities such as exponential growth parameters, which are discussed below.

The H_2-O_2 reaction system, under low-density conditions, has been shown to proceed by well-defined stages of combustion: i.e., 1) induction, 2) transition, 3) partial equilibrium, and 4) full equilibrium. Chain initiation, branching and propagation reactions appear to dominate the induction stage of combustion. The transition stage primarily involves chain branching and propagation and is the region

wherein species concentration spikes and overshoots are observed. Association reactions become important in the partial equilibrium stage of system reaction, and, finally, the full equilibrium stage of combustion occurs when all reaction rates become balanced.

B. Results

Since the hydroxyl radical is the intermediate species most often studied in shock-tube investigations of the H_2-O_2 system [43], we have calculated its behavior in the various stages of H_2 combustion. Generally speaking, direct observation of the other intermediate species has been hampered by a lack of methods having the required sensitivities and response times. The O atom concentrations have been measured, but primarily by methods that involve the presence of CO as a reactant [61]. This technique requires another set of elementary reactions that must be considered before the O atom concentrations can be calculated. The H atom concentrations have recently been measured, but these results appear to suffer from the presence of impurities [62]. The temporal behavior of HO_2 in shock-tube work is not well known.

Throughout most of the induction stage, the HO concentration has an exponential growth rate and may be expressed as:

$$[HO] = [HO]_o \exp(\epsilon t) \tag{16}$$

where t is time and ϵ is the exponential growth parameter that depends upon chain branching, propagation and termination as outlined in Section IV. Jachimowski and Houghton [63] have investigated [HO] in the induction period using incident shock-wave experiments coupled with ultraviolet absorption spectroscopic detection of HO. From their data, they calculated ϵ for a variety of fuel-rich and fuel-lean H_2:O_2:Ar gas mixture at different temperatures. Typically, they identified an induction time corresponding with a detectable level of HO concentration and defined $[HO]_o$ as a pseudo-initial concentration related to the rate of initiation. By rewriting Equation (16) as:

$$\tau\epsilon = \ln [HO]_\tau/[HO]_o \tag{17}$$

they were able to calculate the pseudo-initial hydroxyl concentration, $[HO]_o$, as a function of their graphically measured induction time, τ, exponential growth factor, ϵ, and induction-time-related HO concentration, $[HO]_\tau$.

We have performed several computations involving the induction stage of combustion using Jachimowski and Houghton's initial reaction conditions. In Table 4, we present a comparison of their experimental and our calculated, [HO]-based, exponential growth parameters. A comparison of $\epsilon/[O_2]_o$ versus 1000/T is also provided in Figure 19 to demonstrate the temperature and reactant concentration dependencies of the HO exponential growth parameter.

Getzinger and Schott have examined the partial equilibrium stage of H_2 combustion using HO concentration profiles [64]. In their experiments, they initiated the reaction using incident shock-waves and then followed the progress of the reaction using HO ultraviolet absorption spectroscopy. The partial equilibrium stage of combustion occurs when the reaction cycle reaches a point at which the termolecular association reactions decelerate the overall reaction rate. The result is that the reaction species concentrations remain essentially constant for a protracted time interval. These concentrations may be calculated from a single known concentration once the appropriate equilibrium constant information is known.

Following the experimental measurement of the [HO] profiles for a number of fuel-lean H_2-O_2 mixtures, Getzinger and Schott calculated the temporal behavior of the remaining reaction species using analytic functions describing the partial equilibrium condition. In order to focus on the recombination zone of reaction, they calculated concentrations in terms of a dimensionless reaction progress variable, γ, defined by the equation:

$$\gamma = (N - N_{eq})/(1 - N_{eq}) \tag{18}$$

where N is the instantaneous species concentration and N_{eq} is the species concentration at full-equilibrium. Thus, reaction initiation occurs at $\gamma = 1$ and full-equilibrium is attained at $\gamma = 0$.

We have calculated the temporal behavior of each of the reaction species concentrations as a function of γ for one of the fuel-lean H_2-O_2 mixtures examined by Getzinger and Schott. Our data is presented in Figure 20 and includes a set of points representative of those obtained experimentally for [HO]. The calculated data appears to be almost identical with the measured data.

In addition, we have calculated the temporal behavior of the reaction species number densities for the same H_2:O_2:Ar mixture used above and for a mixture containing no Ar. We show these data in Figures 21 and 22. These figures demonstrate the increased reaction time effect that dilution has on the partial equilibrium stage of combustion. They also show the relation of the partial equilibrium stage of reaction to the other stages of combustion.

VI. REACTION EQUILIBRIUM CALCULATIONS

Another test of the detailed H_2-O_2 mechanism is to determine whether the mechanism can predict the species concentrations once chemical equilibrium is reached. Under adiabatic conditions, this means that certain state and thermodynamic variables are accurately determined. In this section, we compare the long-time equilibrium results of our computations with those obtained using the NASA-LEWIS "Computer Program for Calculation of Complex Chemical Equilibrium Compositions" [65].

The comparison described in this section is between two entirely different computational methods. The NASA-LEWIS Program uses a minimization of Gibbs (or Helmholtz) free-energy technique to derive the composition of the chemical equilibrium mixture, whereas our calculations involve the numerical integration of time-dependent, ordinary differential equations defined by the reaction mechanism contained within Table I. The use of a search routine by the NASA-LEWIS Program to define the reaction species included in their calculation adds generality to the comparison.

We have carried out calculations with both programs to obtain the chemical equilibrium composition of an adiabatic, constant-volume combustion of one atmosphere of stoichiometric hydrogen-air (H_2:O_2:N_2/2:1:4) with an initial temperature of 900°K. A comparison of our computed data is

presented in Table 5. In addition to the reaction species concentrations, the chemical equilibrium mixture density, pressure and temperature are calculated. The excellent correlation between the two sets of computed data substantiates the detailed mechanism of Table 1 as a good description of the reactive system in its approach to chemical equilibrium.

Moreover, the NASA-LEWIS Program calculations are in agreement with our initial assumptions regarding: (1) the inert character of N_2 as a diluent, and (2) the predominant role of neutral species in the H_2-O_2 reactive system. Several NASA-LEWIS Program computations were made in which ionic species and nitrogen-containing reaction species were allowed to participate in the chemical equilibrium mixture. In all situations where the final adiabatic temperature was below $\sim$3000°K, it was found that N_2 remained essentially inert and that ionic species concentrations were negligible.

VII. SUMMARY AND CONCLUSIONS

The principal goal of the work presented in this paper was to determine the accuracy with which a proposed reaction mechanism is able to model the chemistry of the H_2-O_2 reactive system. Since analytical and intuitive interpretations of experimental evidence, coupled with conjecture and supposition, are the common tools used in the construction of a detailed reaction mechanism, we have searched for experimental data relatively free of hydrodynamic and diffuse transport effects against which we could test the proposed mechanism. Although it is not possible to define measurable parameters that are unaffected by gasdynamic interactions, some that are minimally affected include: (1) the reaction induction (delay, ignition) times, (2) the temperature-pressure dependence of the second explosion limit, (3) the rate of reaction above the second explosion limit, (4) the temporal behavior of reaction species, under certain circumstances (i.e., shock tubes).

The elementary reactions most important in determining the ignition properties of the H_2-O_2 system are those involved in chain initiation, branching and propagation. Reaction induction times, which depend on the integrated effect of these reactions, have served as a good test of the mechanism

in this regime. The agreement between experimental and computational ignition delays appears to confirm the set of elementary reactions in its description of the initial reaction phase of the $H_2 - O_2$ system.

More specifically, we have shown that calculations in the high-temperature, low-pressure (HTLP) region of H_2 combustion correlate well with experimental induction times. This region is characterized by strong, single-source or integrated kernel ignition having a sharply defined blast-front. The sharpness and uniformity of this strong ignition implies that timescales for chemical interactions are much shorter than timescales for hydrodynamic interactions and, thus, we might expect good agreement between the calculations and experiment.

However, ignition in the low-temperature, high-pressure (LTHP) region is affected by the coupling of gasdynamics and chemistry. This is demonstrated by the mild, multiple source or multiple-kernel appearance of laser-schlieren experiments. Even though this region represents the worst case for zero-dimensional calculations of induction times, there is good agreement between computed and experimental induction times.

The second explosion limit calculations provide a different kind of test of the $H_2 - O_2$ mechanism. In these calculations, third-body recombination or association reactions are important and compete with the bimolecular chain-branching and propagation reactions. Our calculations were performed for stoichiometric $H_2 - O_2$ mixtures in the slow-reactive zones of the temperature-pressure plane. They show that, for a given pressure, the calculated and measured explosion limits disagree by about 20°K. This discrepancy, however, is understandable when we take into account the fact that the first and second explosion limits are affected by vessel dimensions and materials. In the experimental results shown in Figure 17, there is a contribution to the exponential growth factor, ϵ, of Equation 6 due to chain termination by heterogeneous reactions on the chamber walls. Thus, the need to include heterogeneous reactions indicates an important difference between our mechanism and one necessary for the description of this specific experiment. Nevertheless, these explosion limit calculations have shown the

correct trend of the second explosion limit. The displacement of the calculated results toward lower temperatures is reasonable when the absence of heterogeneous reactions in our mechanism is considered.

An additional test of the mechanism in Table 1 was provided by computations carried out along an isotherm in the slow-reactive zone above the second explosion limit. The appropriate balance between bimolecular chain branching and termolecular chain termination is demonstrated by the calculated results for the overall reaction rate producing H_2O as presented in Figure 18.

Comparisons were also made between calculations and experimental measurements of the temporal behavior of hydroxyl radicals under different reaction conditions found in shock-tube experiments. These HO concentrations were first calculated for the induction period of highly-diluted, H_2-O_2 gas mixtures. Exponential growth factors, ϵ, were calculated for a number of temperatures, pressures, and H_2-O_2-diluent mixture compositions. As shown in Table 4, the experiments and calculations are in good agreement. These tests also help substantiate the chain initiation, branching and propagation parts of the reaction mechanism.

The partial equilibrium stage of H_2 combustion is the region in which termolecular association reactions become important to the deceleration of chain-linked reactions. Here is where the major amount of thermochemical energy release is achieved. The temporal behavior of HO concentrations in this stage was calculated and is shown together with the experimental results in Figure 20. Here, again, good agreement between experiment and computation was obtained. This, as in the second explosion limit calculations, adds support to the validity of the chain termination reactions.

Finally, the proposed reaction mechanism was used to calculate the species concentrations, density, temperature and pressure of a reaction mixture that had reached chemical equilibrium. The good agreement obtained between the results of this calculation and a calculation and a calculation made using the NASA-LENIG Program (which is a technique for calculating equilibrium properties based in

minimization the the free energy) supports the general validity of the proposed reaction mechanism, the reaction rate coefficients, and the species enthalpies.

ACKNOWLEDGMENTS

The authors would like to acknowledge Drs. T.R. Young and M. Flanigan for their help in using CHEMOD. This work has been sponsored by the Naval Research Laboratory through the Office of Naval Research.

REFERENCES

1. M. Flanigan and T.R. Young (manuscript submitted for publication).

2. T.R. Young and J.P. Boris, *J. Phys. Chem.*, **81**, 2424 (1977).

3. H.W. Thompson and C.N. Hinshelwood, *Proc. Roy. Soc. London, Ser. A(122)*, 610 (1929).

4. A.B. Sagulin, *Z. Phys.*, **48**, 571 (1928).

5. A.B. Sagulin, *Z. Phys. Chim. Abt. B*, **1**, 275 (1928).

6. N. Semenov, *Z. Phys.*, **46**, 109 (1927).

7. D. Kopp, A. Kowalsky, A.B. Sagulin and N. Semenov, *Z. Phys. Chim. Abt. B*, **6**, 307 (1930).

8. C.N. Hinshelwood and A.T. Williamson, *The Reaction Between Hydrogen and Oxygen*, Oxford University Press, Oxford (1934).

9. N. Semenov, *Chemical Kinetics and Chain Reactions*, Oxford University Press, Oxford (1935).

10. W. Jost, *Explosion and Combustion Processes in Gases*, McGraw-Hill, New York (1939).

11. B. Lewis and G. von Elbe, *Combustion, Flames and Explosion of Gases*, Cambridge University Press, Cambridge (1938) and Academic Press, New York (1951).

12. G.A. Minkoff and C.F.H. Tipper, *Chemistry of Combustion Reactions*, Butterworths, London (1962).

13. G. Dixon-Lewis and D.J. Williams, *Comprehensive Chemical Kinetics, Vol. 17*, C.H. Bamford and C.F.H. Tipper, Editors, Elsevier Scientific Publishing Co., Amsterdam (1977).

14. C.N. Hinshelwood and E.A. Moelwyn-Hughes, *Proc. Roy. Soc. London*, Ser. A. (138), 311 (1932).

15. a) A.A. Frost and N.H. Alyea, *J. Am. Chem. Soc.*, **55**, 3227 (1933).
    b) Ibid., **56**, 1251 (1934).

16. a) A. Kowalsky, *Phys. Z. Sowjetunion*, **1**, 595 (1932).
    b) Ibid., **4**, 723 (1933).

17. N. Semenova, *Acta Phys. Chim. U.R.S.S.*, **6**, 25 (1937).

18. A. Biron and A. Nalbandjan, *Acta Phys. Chim. U.R.S.S.*, **6**, 43 (1937).

19. a) R.N. Pease, *J. Am. Chem. Soc.*, **52**, 5106 (1930).
    b) Ibid., **53**, 3188 (1931).

20. a) B. Lewis and G. von Elbe, *J. Chem. Phys.*, **9**, 194 (1941).
    b) Ibid., **10**, 366 (1942).

21. A.C. Egerton and D.R. Warren, *Proc. Roy. Soc. London, Ser. A(204)*, 465 (1951).

22. D.R. Warren, *Proc. Roy. Soc. London, Ser A(211)*, 86 (1952).

23. D.R. Stull and H. Prophet, *JANAF Thermochemical Tables*, 2nd edition, Nat. Stand. Ref. Data Ser., Nat. Bur. Stand. No. 37 (1971).

24. V.S. Engleman, *Survey and Evaluation of Kinetic Data on Reactions in Methane/Air Combustion*, Environmental Protection Agency Report No. EPA-600/2-76-003 (1976).

25. T. Asaba, W.C. Gardiner and R.F. Stubbeman, *Tenth Symp. (Int.) on Comb.*, p. 295, Combustion Institute, Pittsburgh (1965).

26. F.E. Belles and M.R. Lauver, *Tenth Symp. (Int.) on Comb.*, p. 285, Combustion institute, Pittsburgh (1965).

27. W.C. Gardiner, Jr., *Acc. Chem. Res.*, **10**, 326 (1977).

28. R. Zellner, *J. Phys. Chem.*, **83**, 18 (1979).

29. K. Shuler, J. Ross and J.C. Light, *Kinetic Processes in Gases and Plasmas*, A.R. Hochstim, editor, Academic Press, New York.

30. R.L. LeRoy, *J. Phys. Chem.*, **73**, 4338 (1969).

31. M. Menzinger and R.L. Wolfgang, *Angew. Chem.*, **81**, 446 (1969).

32. B. Perlmutter-Hayman, *Prog. Inorg. Chem.*, **20** (1976).

33. a) W.R. Schulz and D.J. Le Roy, *J. Chem. Phys.* **42**, 3869 (1965).
b) B.A. Ridley, W.R. Schulz and D.J. Le Roy, ibid, **44**, 3344 (1966).

34. T.C. Clark and J.E. Dove, *Can. J. Chem.*, **51**, 2147 (1973).

35. R.G. Manning and M.J. Kurylo, *J. Phys. Chem.*, **81**, 291 (1977).

36. M.S. Zahniser, B.M. Berquist and F. Kaufman, *Int. J. Chem. Kinet.*, **10**, 5 (1978).

37. J.H. Birely and J.L. Lyman, *J. Photochem.*, **4**, 269 (1975).

38. J.E. Spencer, H. Endo and G.P. Glass, *Sixteenth Symp. (Int.) on Comb.*, p. 829, Combustion Institute, Pittsburgh (1977).

39. D.L. Baulch, D.D. Drysdale, D.G. Horne and A.C. Lloyd, *Evaluated Data for High Temperature Reactions*, Butterworths, London (1972).

40. A. Nalbandjan, *Acta Physicochim U.R.S.S.*, **19**, 483 (1944).

41. N. Semenov, *Acta Physicochim U.R.S.S.*, **20**, 291 (1945).

42. G.L. Schott and J.L. Kinsey, *J. Chem. Phys.*, **29**, 1177 (1958).

43. G.L. Schott and R.W. Getzinger, *Physical Chemistry of Fast Reactions*, **1**, 81, B.P. Levitt, editor, Plenum Press (1973).

44. F.E. Belles and T.A. Brabbs, *Thirteenth Symp. (Int.) on Comb.*, p. 165, Combustion Institute, Pittsburgh (1971).

45. a) H. Mirels, *Phys. Fluids*, **6**, 1201 (1963).
b) Ibid., **9**, 1907 (1966).

46. H. Miyama and T. Takeyama, *J. Chem. Phys.*, **41**, 2287 (1965).

47. R.A. Strehlow and A. Cohen, *Phys. Fluids*, **5**, 97 (1962).

48. S. Fujimoto, *Bull. Chem. Soc. Jpn.*, **36**, 1233 (1963).

49. G.B. Skinner and G.H. Ringrose, *J. Chem. Phys.*, **42**, 2190 (1965).

50. a) S.G. Saytzev and R.I. Soloukhin, *Eighth Symp. (Int.) on Comb.*, p. 344, Williams and Wilkins, Baltimore (1962).
b) V.V. Voevodsky and R.I. Soloukhin, *Tenth Symp. (Int.) on Comb.*, p. 279, Combustion Institute, Pittsburgh (1965).
c) R.I. Soloukhin, *Shock Waves and Detonations in Gases*, Mono Book Corp., Baltimore (1966).

51. a) J.W. Meyer and A.K. Oppenheim, *Thirteenth Symp. (Int.) on Comb.*, p. 1153, Combustion Institute, Pittsburgh (1971).

b) J.W. Meyer and A.K. Oppenheim, *Comb. and Flame*, 17, 65 (1971).

52. R.S. Brokaw, *Tenth Symp. (Int.) on Comb.*, p. 269, Combustion Institute, Pittsburgh (1965).

53. C.B. Wakefield, D.L. Ripley and W.C. Gardiner, Jr., *J. Chem. Phys.*, **50**, 325 (1969).

54. D.R. White, *Eleventh Symp. (Int.) on Comb.*, p. 147, Combustion Institute, Pittsburgh (1969).

55. E.P. Dougherty and H. Rabitz (in press, *J. Chem. Phys.*).

56. D.B. Ripley and W.C. Gardiner, Jr., *J. Chem. Phys.*, **44(6)**, p. 2285 (1966).

57. R.W. Getzinger, *Eleventh Symp. (Int.) on Comb.*, p 117, Combustion Institute, Pittsburgh (1967).

58. R.R. Baldwin, M.E. Fuller, J.S. Hillman, D. Jackson and R.W. Walker, *J. Chem. Soc., Faraday Trans.*, **1(70)**, p. 635 (1974).

59. M.W. Slack, *Combustion and Flame*, **28**, p. 241 (1977).

60. G. von Elbe and B. Lewis, *J. Chem. Phys.*, **9**, p. 194 (1941).

61. A.M. Dean, D.C. Steiner and E.E. Wang, *Combustion and Flame*, **32**, p. 73 (1978).

62. C.C. Chiang and G.B. Skinner, "Shock Tubes and Waves: Proceedinges of the XII International Symposium on Shock Tubes and Waves," pp. 629-639, University of Washington Press (1980).

63. C.J. Jachimowski and W.M. Houghton, *Combustion and Flame*, **17**, p. 25 (1971).

64. R.W. Getzinger and G.L. Schott, *J. Chem. Phys.*, **43(9)**, p. 3237 (1965).

65. S. Gordon and B.J. McBride, "Computer Program for Calculation of Complex Chemical Equilibrium Compositions, Rocket Performance, Incidental and Reflected Shocks, and Chapman-Jouquet Deformations," NASA SP-273, NASA, Washington, D.C. (1976).

66. D.R. Jenkins, V.S. Yumlu and D.B. Spalding, *Eleventh Symp. (Int.) on Comb.*, p. 779, Combustion Institute, Pittsburgh (1967).

67. J.P. Longwell and M.A. Weiss, *Ind. Eng. Chem.*, **47**, p. 1634 (1955).

68. R.F. Sawyer and I. Glassman, *Twelfth Symp. (Int.) on Combustion*, p. 469, Combustion Institute, Pittsburgh (1969).

Table 1. $H_2 - O_2$ Elementary Reaction Mechanism.

i	Reaction	$k_i = AT^B \exp(-C/T)$[a]			Source
		A[b]	B	C[b]	
1	$H + HO \rightleftharpoons O + H_2$	1.40(−14)	1.00	3.50(+03)	Baulch et al., 1972
−1		3.00(−14)	1.00	4.48(+03)	Baulch et al., 1972
2	$H + HO_2 \rightleftharpoons H_2 + O_2$	4.20(−11)	0.00	3.50(+02)	Baulch et al., 1972
−2		9.10(−11)	0.00	2.91(+04)	Baulch et al., 1972
3	$H + HO_2 \rightleftharpoons HO + HO$	4.20(−10)	0.00	9.50(+-2)	Baulch et al., 1972
−3		2.00(−11)	0.00	2.02(+04)	Baulch et al., 1972
4	$H + H_2 \rightleftharpoons O + H_2O$	8.30(−11)	0.00	5.00(+02)	Hampson, 1973
−4		1.75(−12)	0.45	2.84(+04)	$k_r = k_f/K_c$
5	$H + H_2O_2 \rightleftharpoons HO_2 + H_2$	2.80(−12)	0.00	1.90(+03)	Baulch et al., 1972
−5		1.20(−12)	0.00	9.40(+03)	Baulch et al., 1972
6	$H + H_2O_2 \rightleftharpoons HO + H_2O$	5.28(−10)	0.00	4.50(+03)	Baulch et al., 1972
−6		3.99(−10)	0.00	4.05(+04)	$k_r = k_f/K_c$
7	$H + O_2 \rightleftharpoons HO + O_2$	2.70(−11)	0.00	0.00(+00)	Hampson, 1973
−7		5.20(−15)	0.69	3.86(+04)	$k_r = k_f/K_c$
8	$HO + H_2 \rightleftharpoons H + H_2O$	1.83(−15)	1.30	1.84(+03)	Cohen and Westberg, 1978
−8		1.79(−14)	1.20	9.61(+03)	Cohen and Westberg, 1978
9	$HO + HO \rightleftharpoons H_2 + O_2$	1.09(−13)	0.26	1.47(+04)	$k_f = k_r K_c$
−9		2.82(−11)	0.00	2.42(+04)	Olson, 1977
10	$HO + HO \rightleftharpoons O + H_2O$	1.00(−16)	1.30	0.00(+00)	Cohen and Westberg, 1978
−10		3.20(−15)	1.16	8.77(+03)	$k_r = k_f/K_c$
11	$HO + HO_2 \rightleftharpoons H_2O + O_2$	8.30(−11)	0.00	5.03(+02)	Lloyd, 1974
−11		2.38(−10)	0.17	3.69(+04)	$k_r = k_f/K_c$
12	$HO + H_2O_2 \rightleftharpoons HO_2 + H_2$	1.70(−11)	0.00	9.10(+02)	Baulch et al., 1972
−12		4.70(−11)	0.00	1.65(+04)	Baulch et al., 1972
13	$HO + O_3 \rightleftharpoons HO_2 + O_2$	1.60(−12)	0.00	9.56(+02)	Hampson, 1973
−13		6.69(−14)	0.33	2.04(+04)	$k_r = k_f/K_c$
14	$HO_2 + H_2 \rightleftharpoons HO + H_2O$	1.20(−12)	0.00	9.41(+03)	Olson, 1977
−14		1.33(−14)	0.43	3.62(+04)	$k_r = k_f/K_c$
15	$HO_2 + HO_2 \rightleftharpoons H_2O_2 + O_2$	3.00(−11)	0.00	5.00(+02)	Hampson, 1973
−15		1.57(−09)	−0.38	2.20(+04)	$k_r = k_f/K_c$

Table 1 (Continued). $H_2 - O_2$ Elementary Reaction Mechanism.

i	Reaction	$k_r = AT^B \exp(-C/T)$[a]			Source
		A[b]	B	C[b]	
16	$HO_2 + O_3 \rightleftharpoons HO + 2O_2$	1.70(−13)	0.00	1.41(+03)	Lloyd, 1974
−16		9.94(−46)	0.16	1.60(+04)	$k_r = k_f/K_c$
17	$O + HO \rightleftharpoons H + O_2$	2.72(−12)	0.28	−8.10(+01)	$k_f = k_r K_c$
−17		3.70(−10)	0.00	8.45(+03)	Baulch et al., 1972
18	$O + HO_2 \rightleftharpoons HO + O_2$	8.32(−11)	0.00	5.03(+02)	Lloyd, 1974
−18		2.20(−11)	0.18	2.82(+04)	$k_r = k_f/K_c$
19	$O + H_2O_2 \rightleftharpoons H_2O + O_2$	1.40(−12)	0.00	2.12(+03)	Hampson, 1973
−19		5.70(−14)	0.52	4.48(+04)	$k_r = k_f/K_c$
20	$O + H_2O_2 \rightleftharpoons HO + HO_2$	1.40(−12)	0.00	2.13(+03)	Hampson, 1973
−20		2.07(−15)	0.64	8.23(+03)	$k_r = k_f/K_c$
21	$O + O_3 \rightleftharpoons O_2 + O_2$	1.89(−11)	0.00	2.30(+03)	Hampson, 1973
−21		1.98(−11)	0.00	5.06(+04)	$k_r = k_f/K_c$
22	$H + H + M \rightleftharpoons H_2 + M$	1.80(−30)	−1.00	0.00(+00)	Baulch et al., 1972
−22		3.70(−10)	0.00	4.83(−04)	Baulch et al., 1972
23	$H + HO + M \rightleftharpoons H_2O + M$	6.20(−26)	−2.00	0.00(+00)	Baulch et al., 1972
−23		5.80(−09)	0.00	5.29(+04)	Baulch et al., 1972
24	$H + O_2 + M \rightleftharpoons HO_2 + M$	4.14(−33)	0.00	−5.00(+02)	Baulch et al., 1972
−24		3.50(−09)	0.00	2.30(+04)	Baulch et al., 1972
25	$HO + HO + M \rightleftharpoons H_2O_2 + M$	2.50(−33)	0.00	−2.55(+03)	Baulch et al., 1972
−25		2.00(−07)	0.00	2.29(+04)	Baulch et al., 1972
26	$O + H + M \rightleftharpoons HO + M$	8.28(−29)	−1.00	0.00(+00)	Bahn, 1969
−26		2.33(−10)	0.21	5.10(+04)	$k_r = k_f/K_c$
27	$O + HO + M \rightleftharpoons HO_2 + M$	2.80(−31)	0.00	0.00(+00)	Bahn, 1969
−27		1.10(−04)	−0.43	3.22(+04)	$k_r = k_f/K_c$
28	$O + O + M \rightleftharpoons O_2 + M$	5.20(−35)	0.00	−9.00(+02)	Baulch et al., 1972
−28		3.00(−06)	−1.00	5.94(+04)	Baulch et al., 1972
29	$O + O_2 + M \rightleftharpoons O_3 + M$	3.31(−35)	0.00	−9.80(+02)	$k_f = k_r K_c$
−29		7.16(−10)	0.00	1.12(+04)	Heimerl, 1979

[a] Bimolecular reaction rate constants are given in units of cm^3/(molecule sec).

[b] Exponentials to the base 10 are given in parenthesis; i.e., $1.00(-10) = 1.00 \times 10^{-10}$.

Table 2. H_2–O_2 Elementary Reaction Equilibrium Constants[a]

i[b]	$K_i = k_f/k_r = A_{eq}T^{B_{eq}} \exp(C_{eq}/T)$[c]		
	A_{eq}	B_{eq}	C_{eq}
1	6.13(−01)	−3.99(−02)	9.67(+02)
2	5.52(+00)	−3.30(−01)	2.86(+04)
3	3.32(+03)	−6.89(−01)	1.89(+04)
4	1.13(+02)	−5.55(−01)	2.76(+04)
5	3.46(+02)	−6.57(−01)	7.09(+03)
6	1.68(+05)	−1.30(+00)	3.37(+04)
7	7.88(+04)	−1.02(+00)	3.83(+04)
8	5.09(−02)	1.84(−01)	7.80(+03)
9	1.67(−01)	3.60(−01)	9.66(+03)
10	3.12(−02)	1.44(−01)	8.77(+03)
11	3.53(−01)	−1.73(−01)	3.63(+04)
12	3.34(+01)	−5.55(−01)	1.48(+04)
13	2.30(+02)	−3.29(−01)	1.94(+04)
14	1.78(+02)	−5.11(−01)	2.66(+04)
15	1.08(−02)	3.77(−01)	2.15(+04)
16	1.71(+31)	−1.62(−01)	1.46(+04)
17	2.72(−03)	3.99(−01)	8.69(+03)
18	9.55(+00)	−2.96(−01)	2.75(+04)
19	4.06(−02)	5.20(−01)	4.27(+04)
20	6.76(+02)	−6.40(−01)	6.10(+03)
21	2.63(+02)	−6.48(−01)	4.69(+04)
22	1.80(−24)	−1.71(−01)	5.22(+04)
23	9.15(−26)	1.30(−02)	6.00(+04)
24	3.41(−25)	1.53(−01)	2.36(+04)
25	1.36(−29)	8.95(−01)	2.60(+04)
26	2.94(−24)	−1.31(−01)	5.12(+04)
27	8.92(−28)	5.57(−01)	3.23(+04)
28	1.03(−26)	2.38(−01)	5.99(+04)
29	2.66(−28)	6.54(−01)	1.28(+04)

[a] Equilibrium constants are given in the non-Arrhenius format used for the individual reaction rate constants and are computed to cover the 300-3000 °K range

[b] "i" refers to the reaction index of Table 1

[c] K_i is given as the concentration based equilibrium constant (K_c) and is dimensionless except for equilibria involving association-dissociation where it is given the units of cm^3/molecule

Table 3. Fuel-Lean Induction Times in the high-temperature, low-pressure (HTLP) Region.

Test No.	Initial Mixture Composition (Moles/Liter)[a]			Initial Temperature (°K)	Reaction Induction Times τ_i (μsec)	
	$[H_2]$	$[O_2]$	[Ar]		Expt.[b]	Calc.[c]
1	2.99(−4)	9.67(−3)	0	1200	51	50
2	2.99(−4)	9.67(−3)	0	1600	8	11
3	2.99(−4)	9.67(−3)	0	2000	2.5	4
4	7.48(−5)	2.99(−4)	9.60(−3)	1200	580	455
5	7.48(−5)	2.99(−4)	9.60(−3)	1600	88	84
6	1.50(−4)	5.98(−4)	9.22(−3)	1600	44	43
7	1.50(−4)	5.98(−4)	9.22(−3)	2000	14	16

(a) Exponentials to the base 10 are given in parentheses i.e., $1.00(-10) = 1.00 \times 10^{-10}$

(b) Experimental data were obtained from the correlation function of the incident shock data published by D.R. White [54]

(c) Calculated data presents τ_i as the time at which the H atom concentration reached a maximum.

Table 4. Induction Zone Exponential Growth Parameters for [HO].

H_2:O_2:Ar	Temperature (°K)	Pressure (atm)	$\tau\epsilon$	
			Calc[a]	Expt[b]
4:1:95	1140	0.62	11.88	11.31
	1840	0.57	5.56	6.05
3:3:94	1124	0.62	10.54	11.72
	1780	0.27	6.00	4.46
1:4:95	1165	0.64	9.72	13.96
	1802	0.28	5.72	6.16
1:8:91	1230	0.72	8.55	10.53
	1700	0.27	5.58	5.84

[a] Induction times, τ_i, were calculated using Jachimowski and Houghton's criterion of $[HO] = 1.0 \times 10^{-7}$ mole/liter to determine the end of the induction period.

[b] Jachimowski and Houghton have estimated the experimental error in $\tau\epsilon$ to be about 10.

Table 5. Comparison of Chemical Equilibrium Compositions obtained by Calculation.

Variable	NASA[a]	Mechanism[b]
$\bar{X}$ (Mole Fraction)		
H_2	4.82(−02)[c]	4.81(−02)[c]
O_2	1.86(−02)	1.75(−02)
H	2.38(−02)	2.29(−02)
O	8.98(−03)	8.22(−03)
HO	2.77(−02)	2.86(−02)
HO_2	1.60(−06)	1.34(−06)
H_2O	2.42(−01)	2.48(−01)
H_2O_2	1.11(−07)	7.28(−08)
O_3	3.62(−10)	2.60(−10)
ρ(g/cm^3)	1.43(−05)	1.45(−05)
P(atm)	1.31(−01)	1.33(−01)
T (°K)	2607	2634

(a) Data computed using Gordon and McBride modification of NASA Program.

(b) Data calculated using detailed mechanism of Table 1 to generate time-dependent ordinary differential equations.

(c) Read tabulated data in scientific notation as: 1.00(−01) = 1.00×10^{-01}

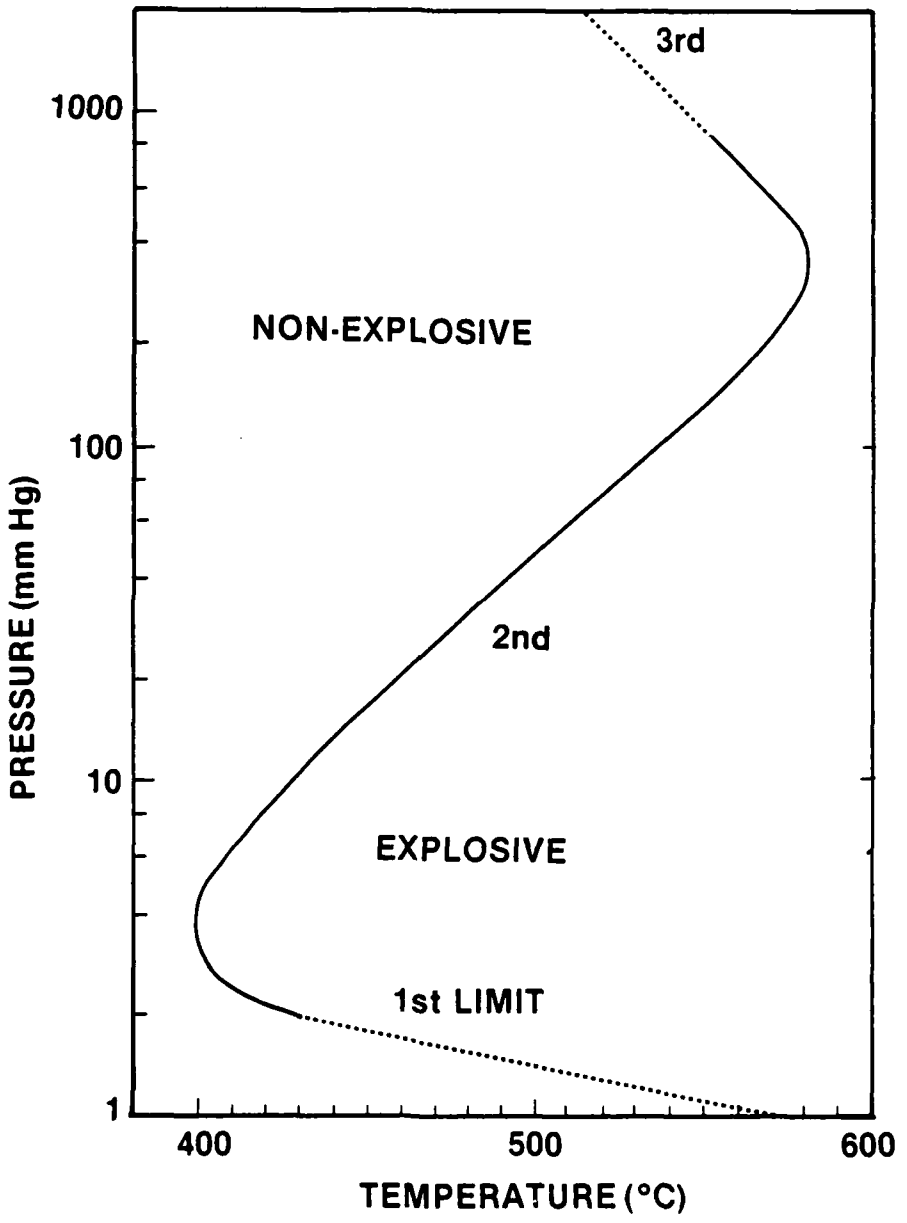

Fig. 1 — Explosion limits for a H_2:O_2 2:1 gas mixture in a KCl-coated static flow reaction bulb. (Adapted from Reference 11.)

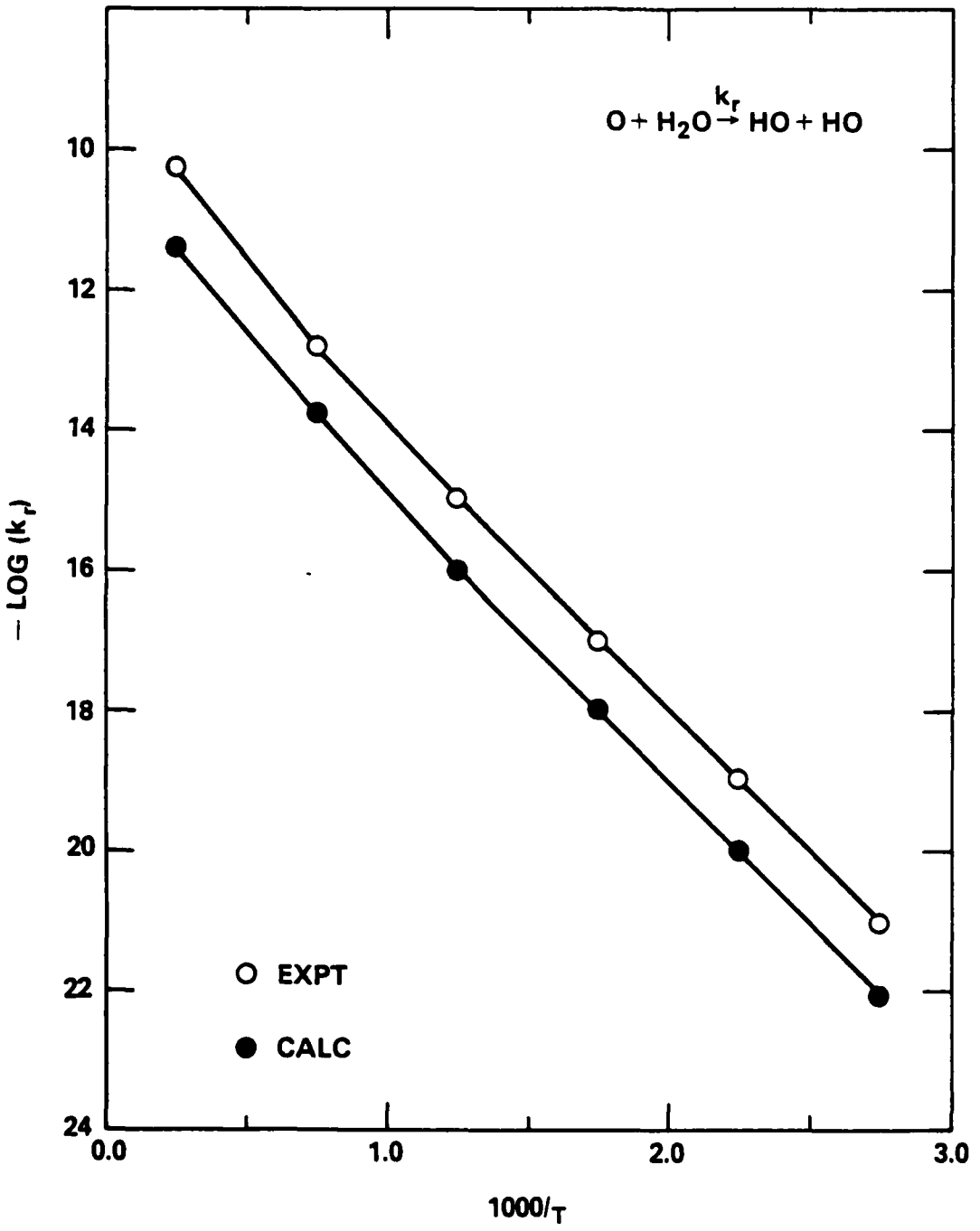

Fig. 2 — Comparison of calculated and experimental reaction rate coefficients for $H_2O_2 + O_2 \rightarrow HO_2 + HO_2$

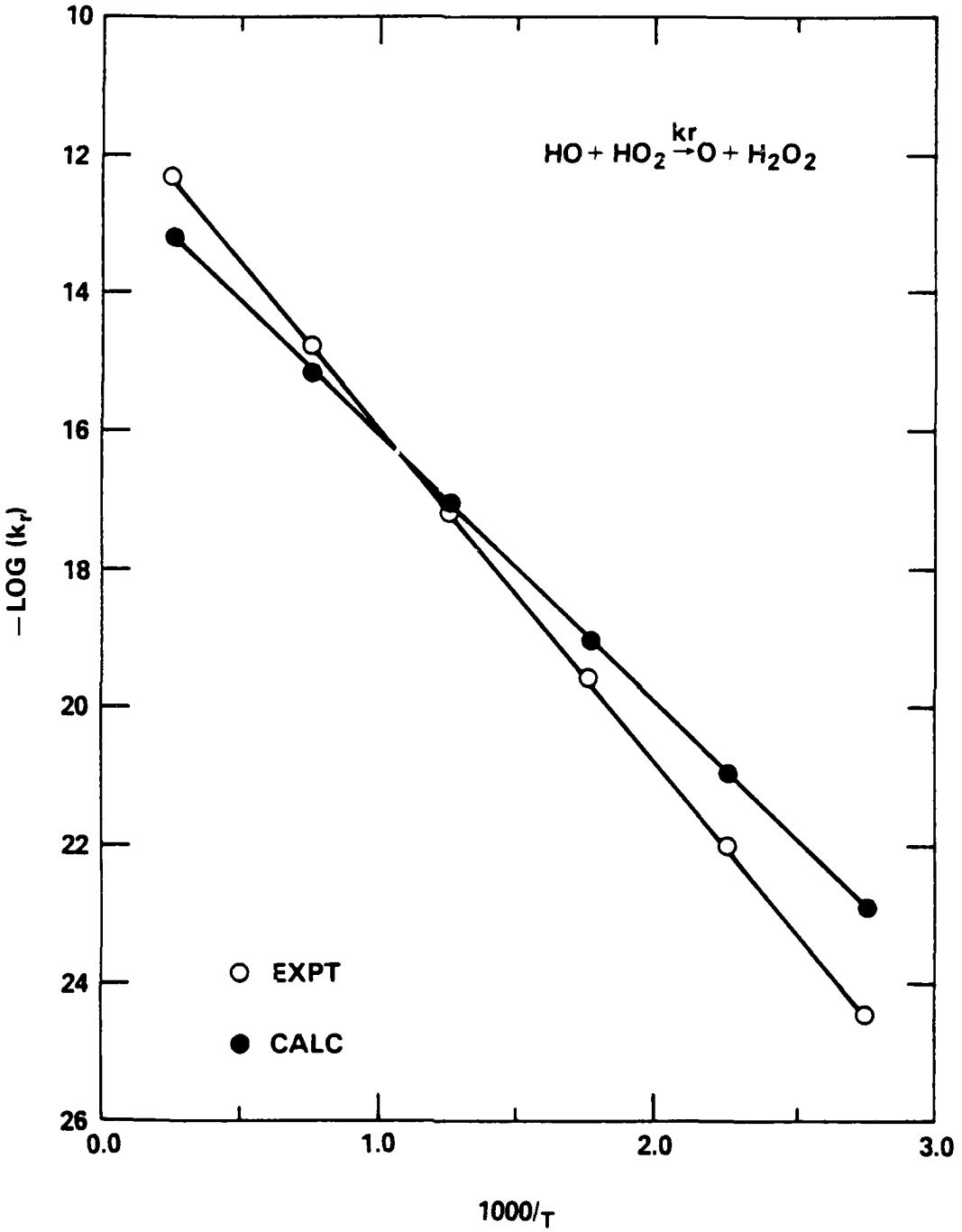

Fig. 3 — Comparison of calculated and experimental reaction rate coefficients for $HO + HO_2 \rightarrow O + H_2O_2$

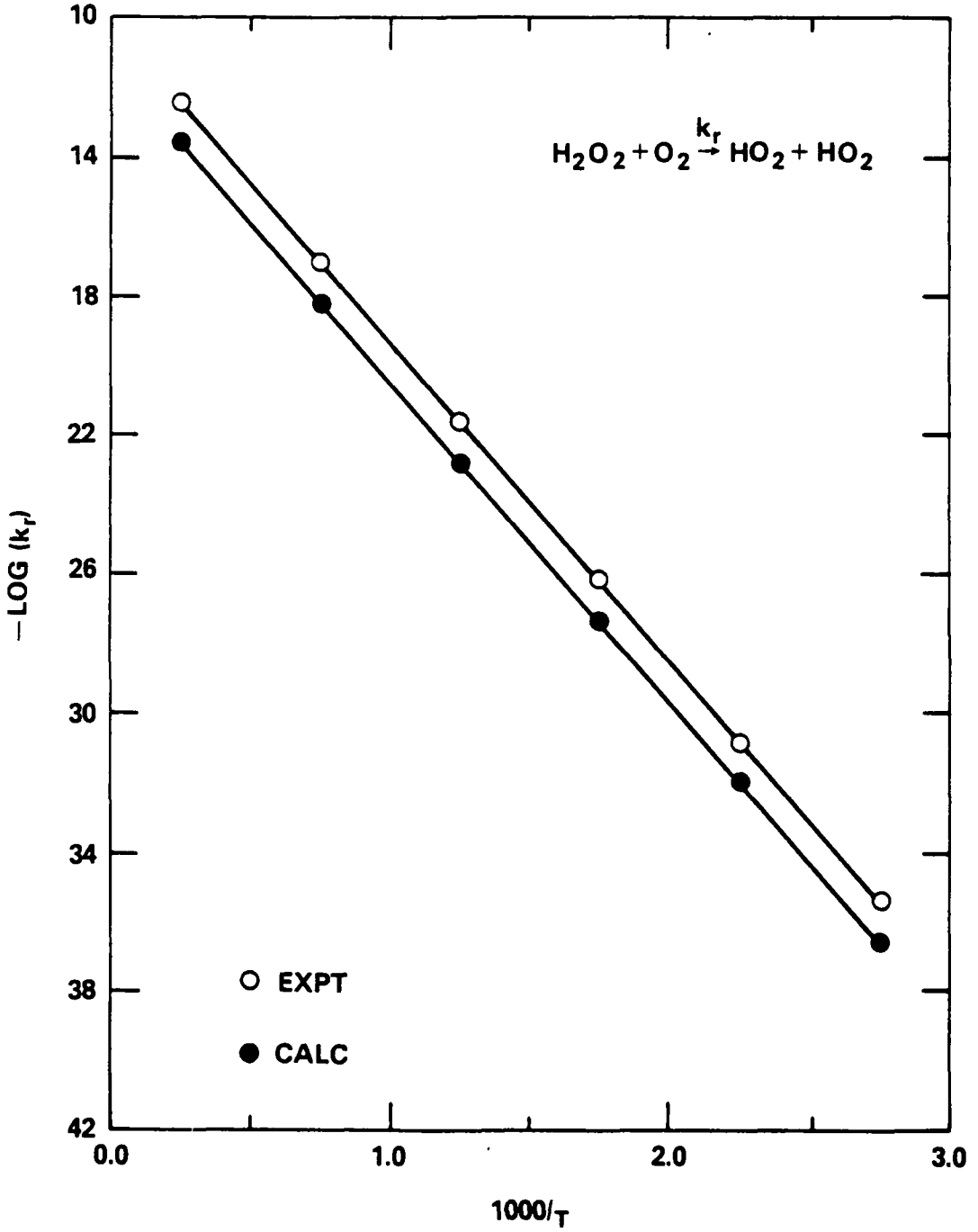

Fig. 4 — Comparison of calculated and experimental reaction rate coefficients for $O + H_2O \rightarrow HO + HO$

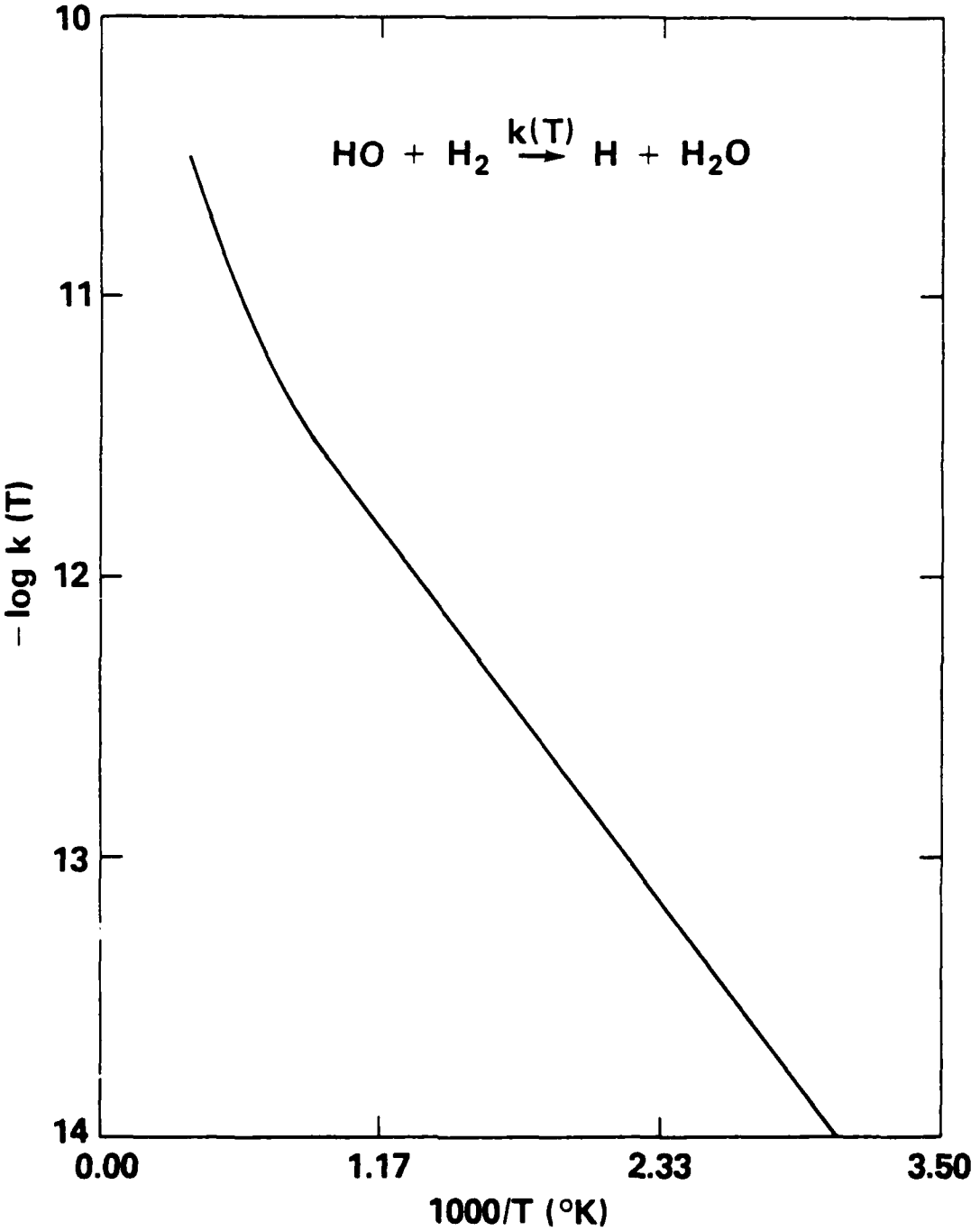

Fig. 5 — Arrhenius plot demonstrating the nonlinear behavior of the HO + H_2 → H + H_2O reaction rate coefficient with temperature

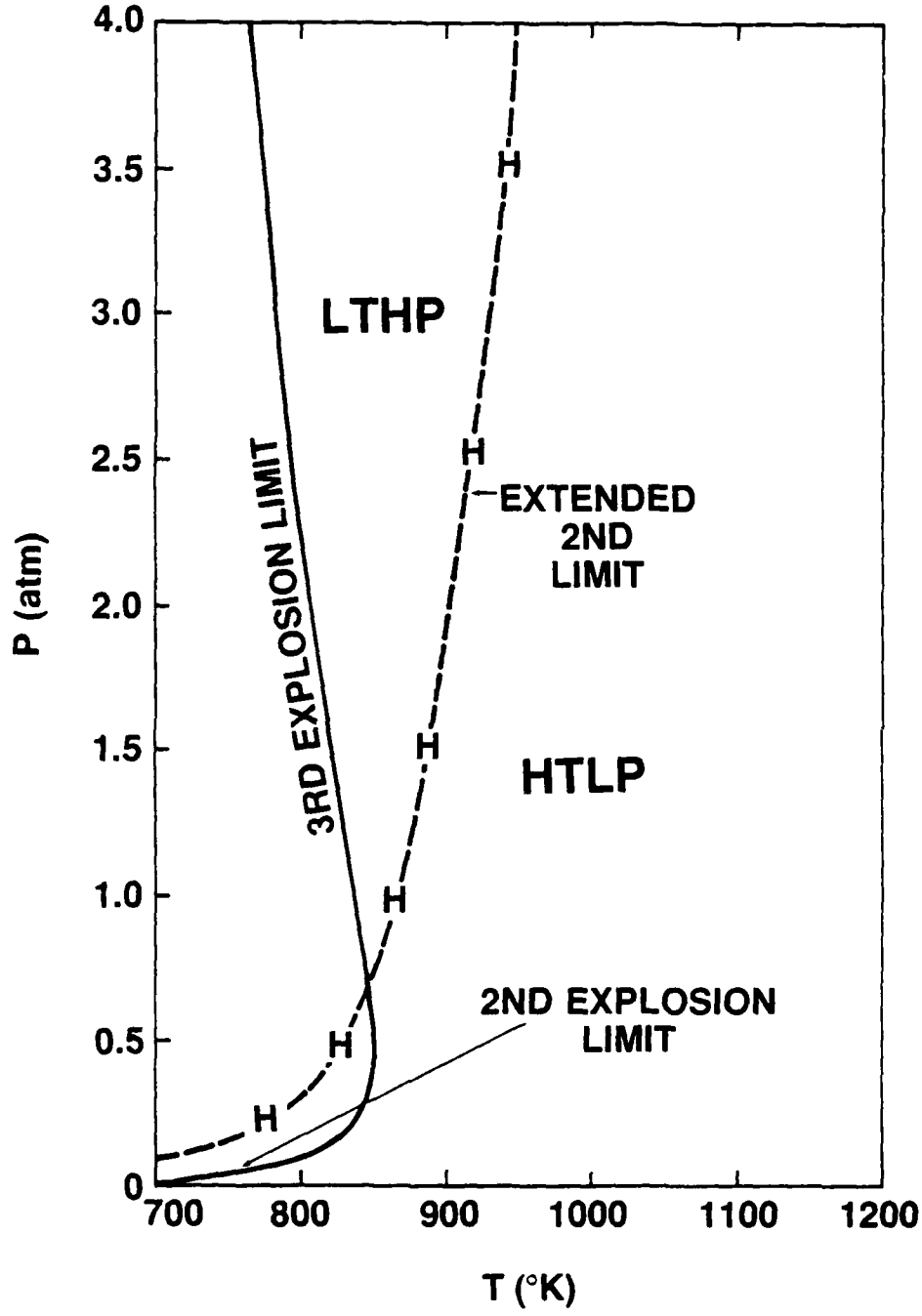

Fig. 6 — The extended 2nd limit defining the LTHP and HTLP regions. (The solid line represents the experimentally observed turnover between the 2nd and 3rd explosion limits and the dashed curve is calculated using the "2nd limit condition.")

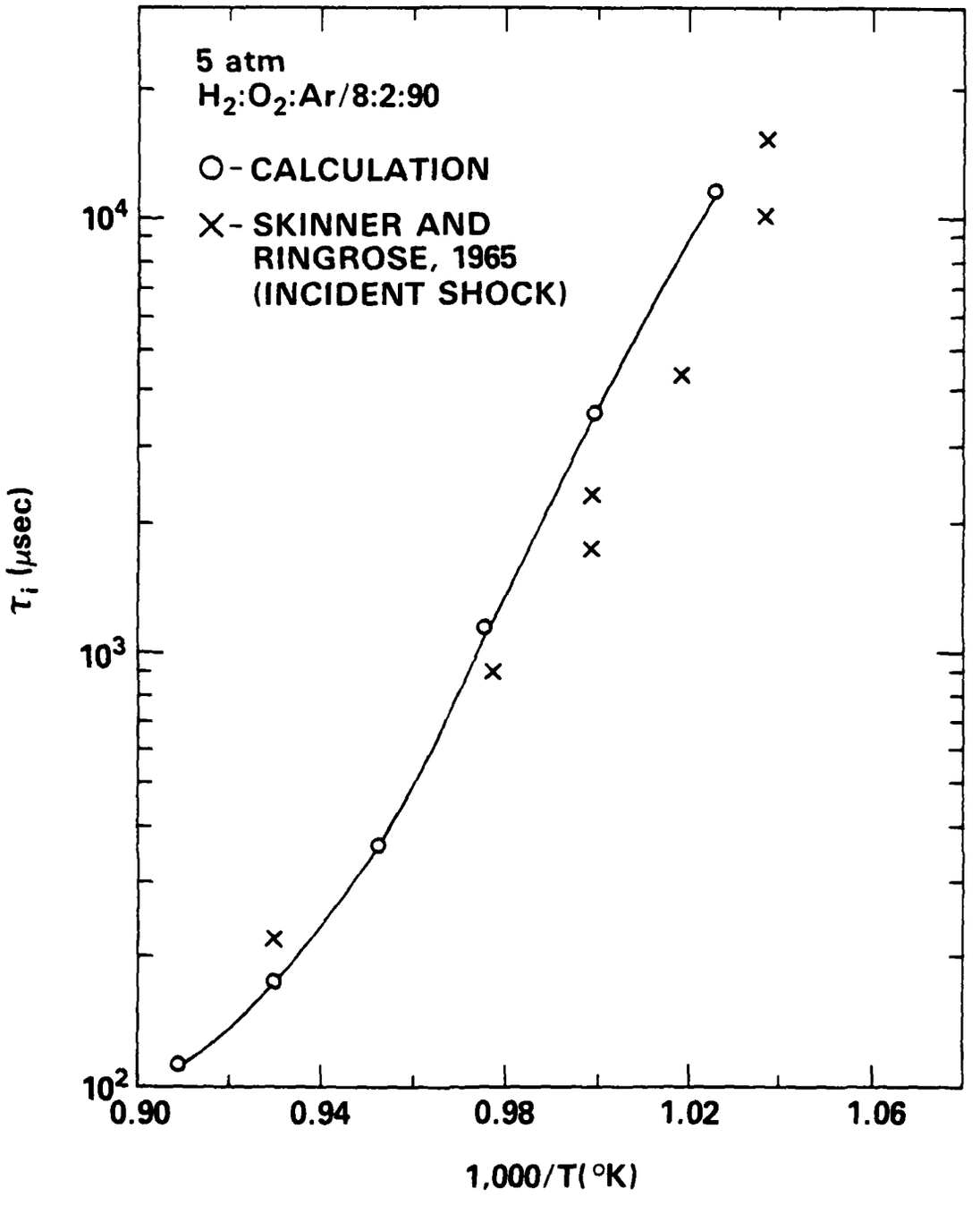

Fig. 7 — Comparison of computed and experimental reaction induction times, τ_i, in the HPLT ignition region for a *dilute, fuel-rich* $H_2 - O_2$ gas mixture. (The solid line connects calculated values. Each circle and cross represent a separate experiment.)

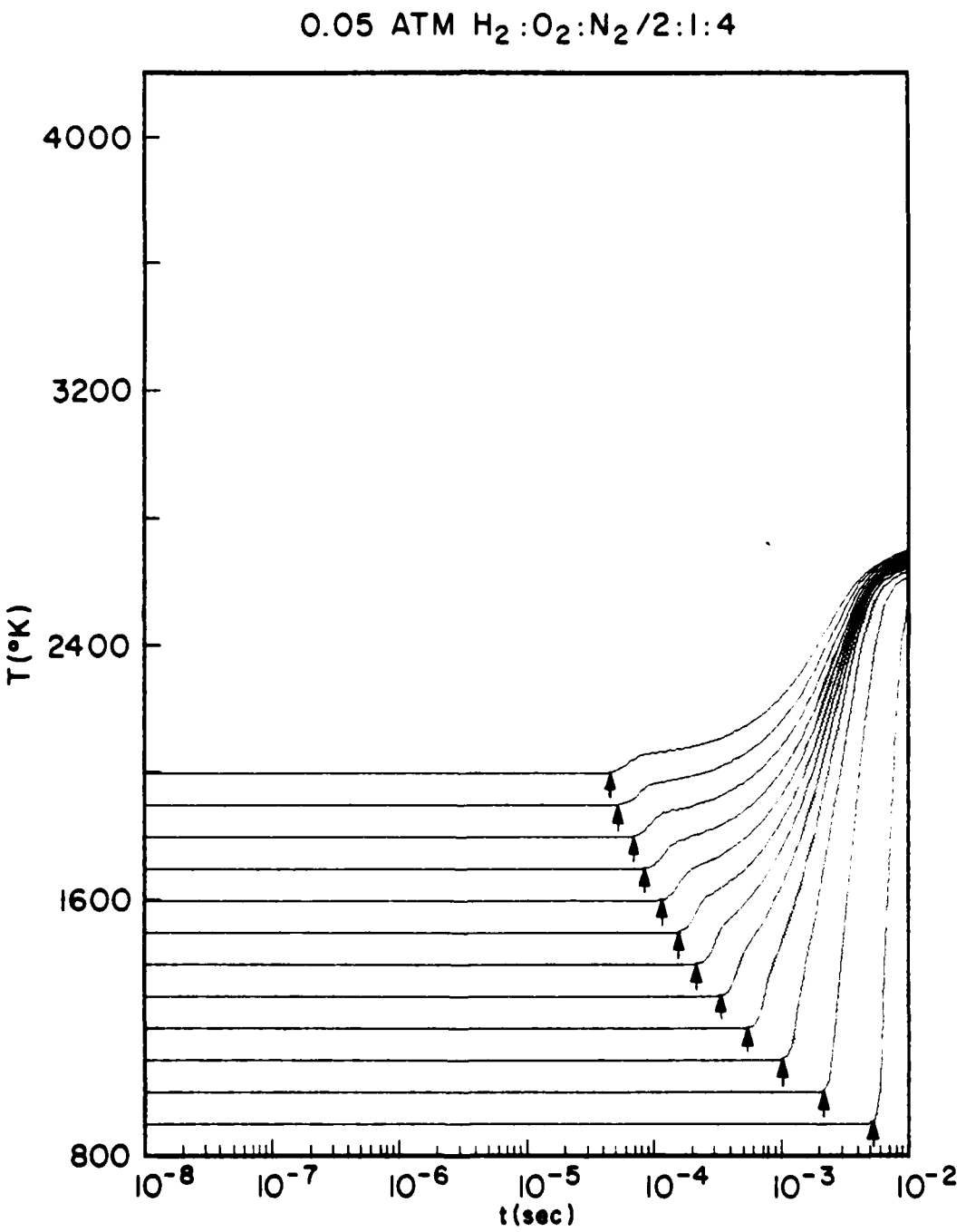

Fig. 8 — Calculated adiabatic temperature profiles for a constant-volume reaction of 0.05 atm of H_2:O_2:N_2 2:1:4 at initial temperatures from 900 to 2000 °K

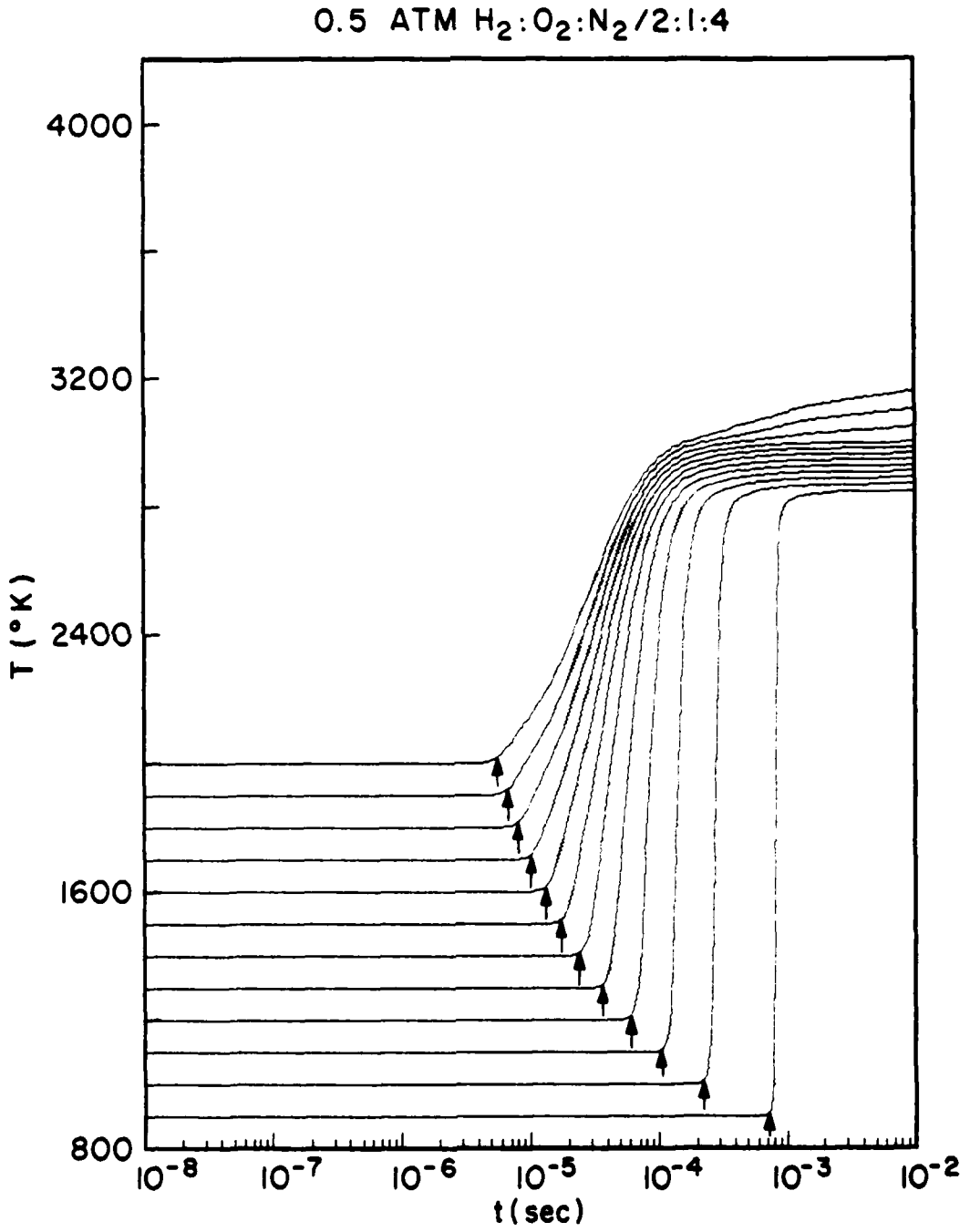

Fig. 9 — Calculated adiabatic temperature profiles for a constant-volume reaction of 0.5 atm of H_2:O_2:N_2 2:1:4 at initial temperatures of 900 to 2000 °K

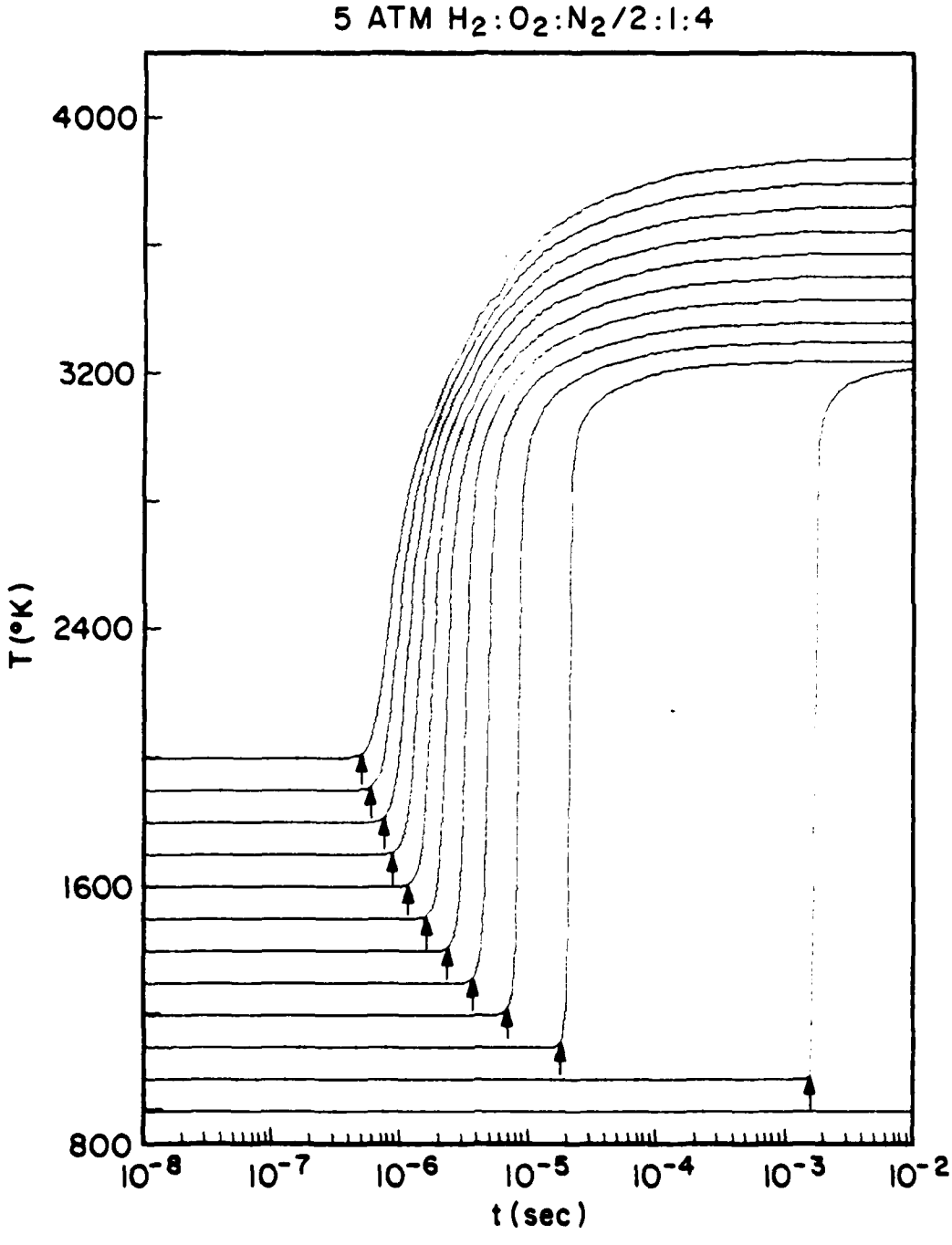

Fig. 10 — Calculated adiabatic temperature profiles for a constant-volume reaction of 5 atm of H_2:O_2:N_2 2:1:4 at initial temperatures of 900 to 2000°K

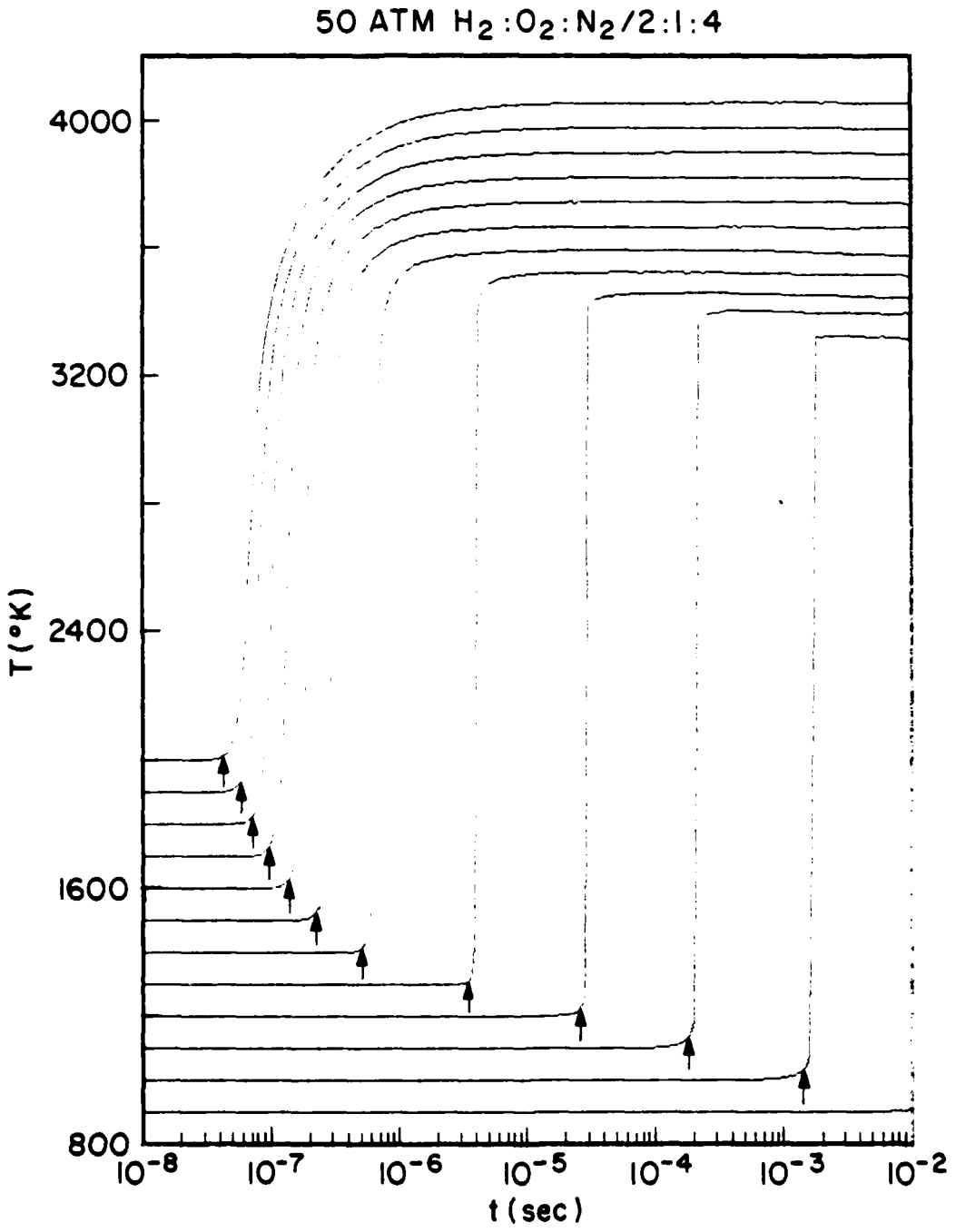

Fig. 11 — Calculated adiabatic temperature profiles for a constant-volume reaction of 50 atm of H_2:O_2:N_2 2:1:4 at initial temperatures of 900 to 2000 °K

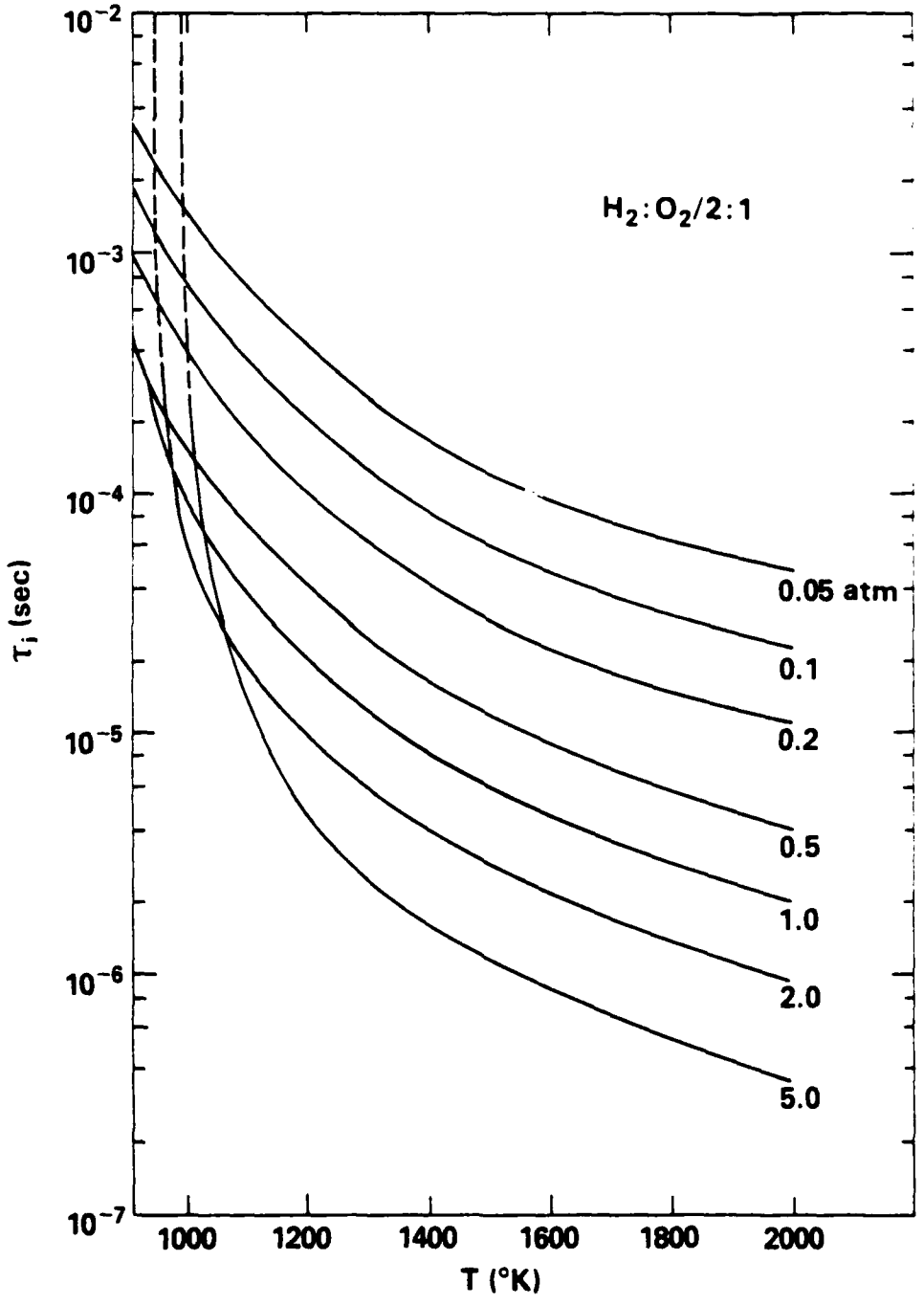

Fig. 12 — Computed isobaric contours of reaction induction time, τ_i, as a function of temperature, T, for H_2:O_2 2:1 gas mixtures

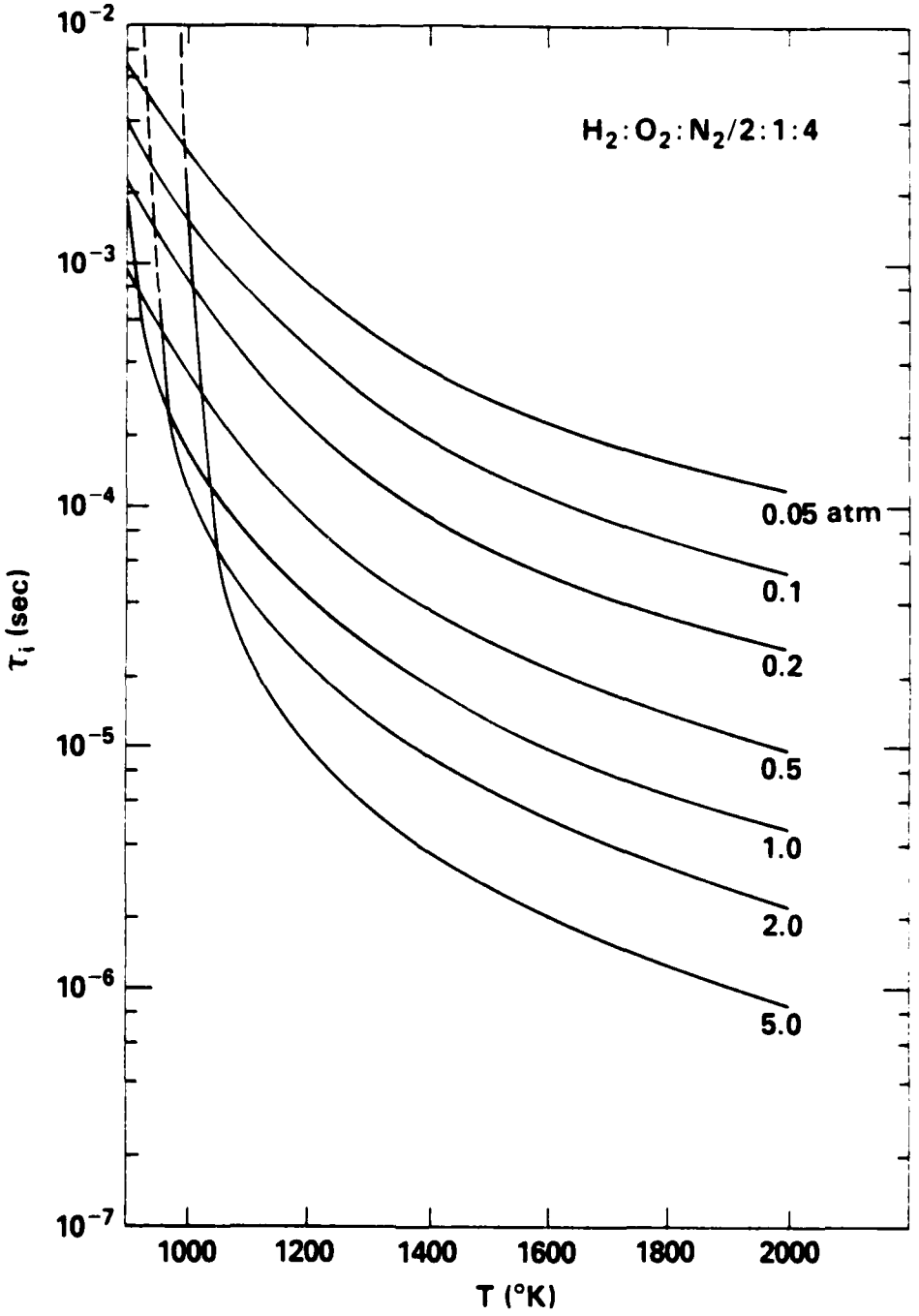

Fig. 13 — Computed isobaric contours of reaction induction time, τ_i, as a function of temperature, T, for H_2:O_2:N_2/2:1:4 gas mixtures

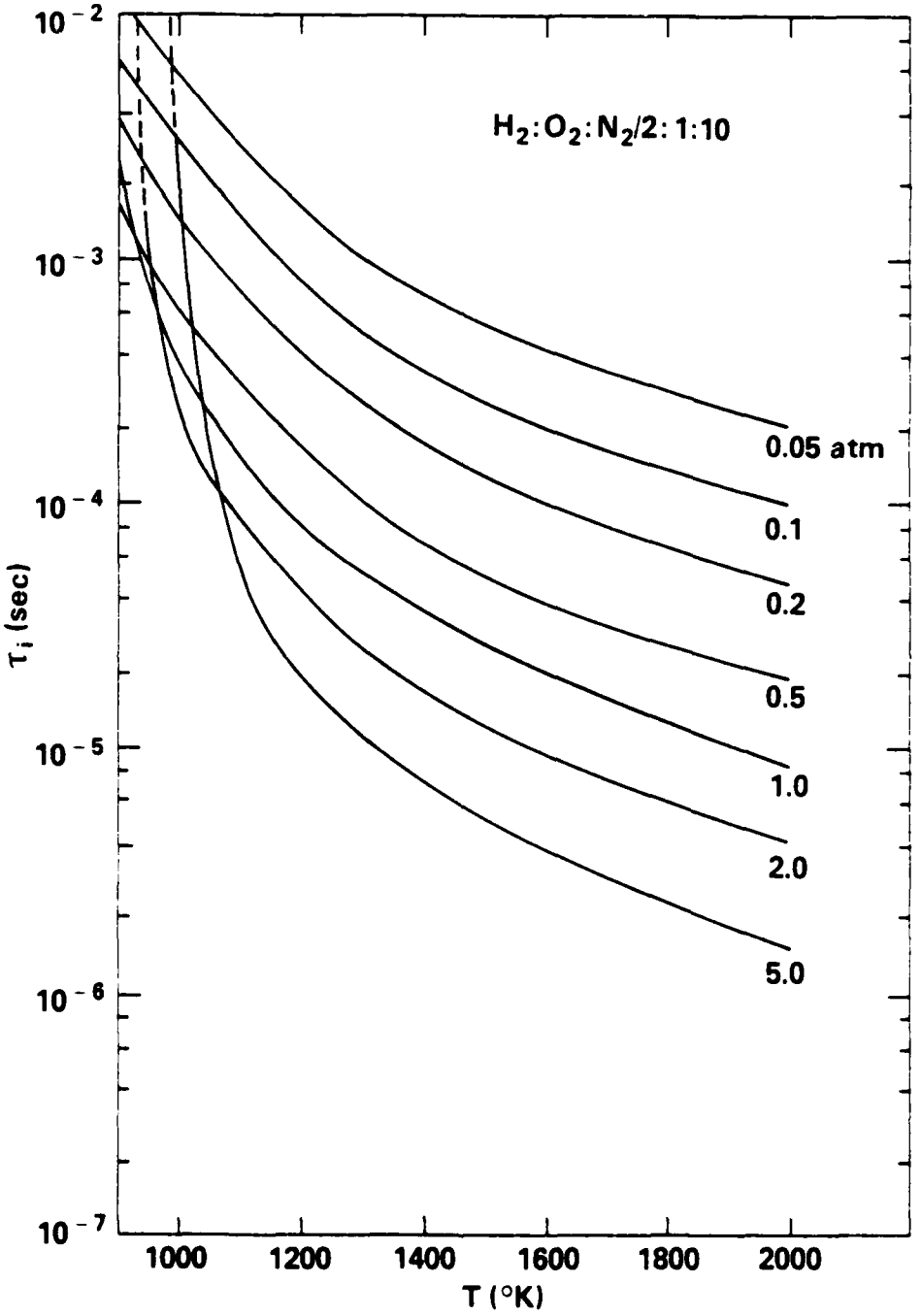

Fig. 14 — Computed isobaric contours of reaction induction time, τ_i, as a function of temperature, T, for $H_2:O_2:N_2$ 2:1:10 gas mixtures

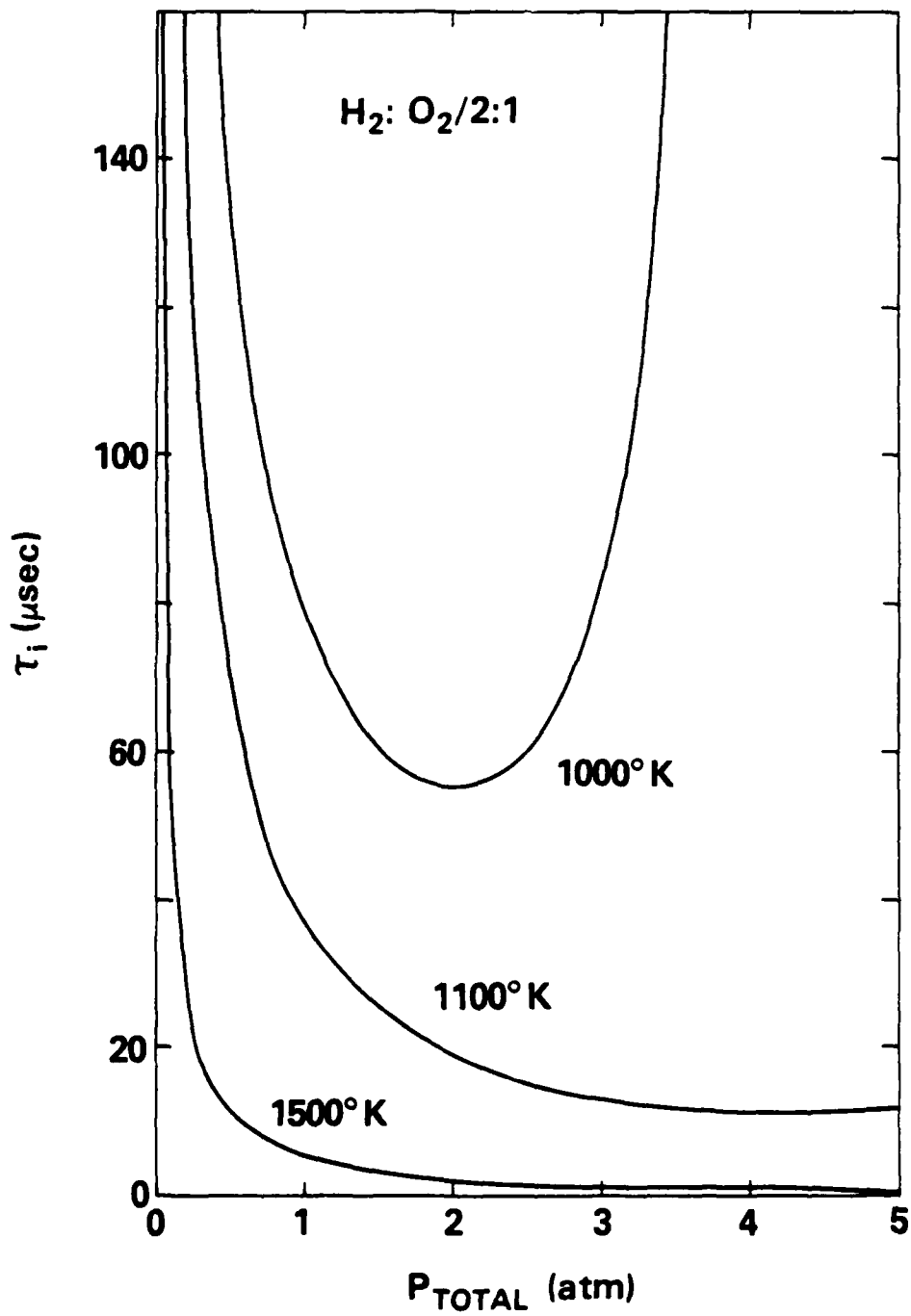

Fig. 15 – Computed isothermal contours of reaction induction time, τ_i, as a function of pressure, P_{TOTAL}, for a stoichiometric $H_2 - O_2$ gas mixture

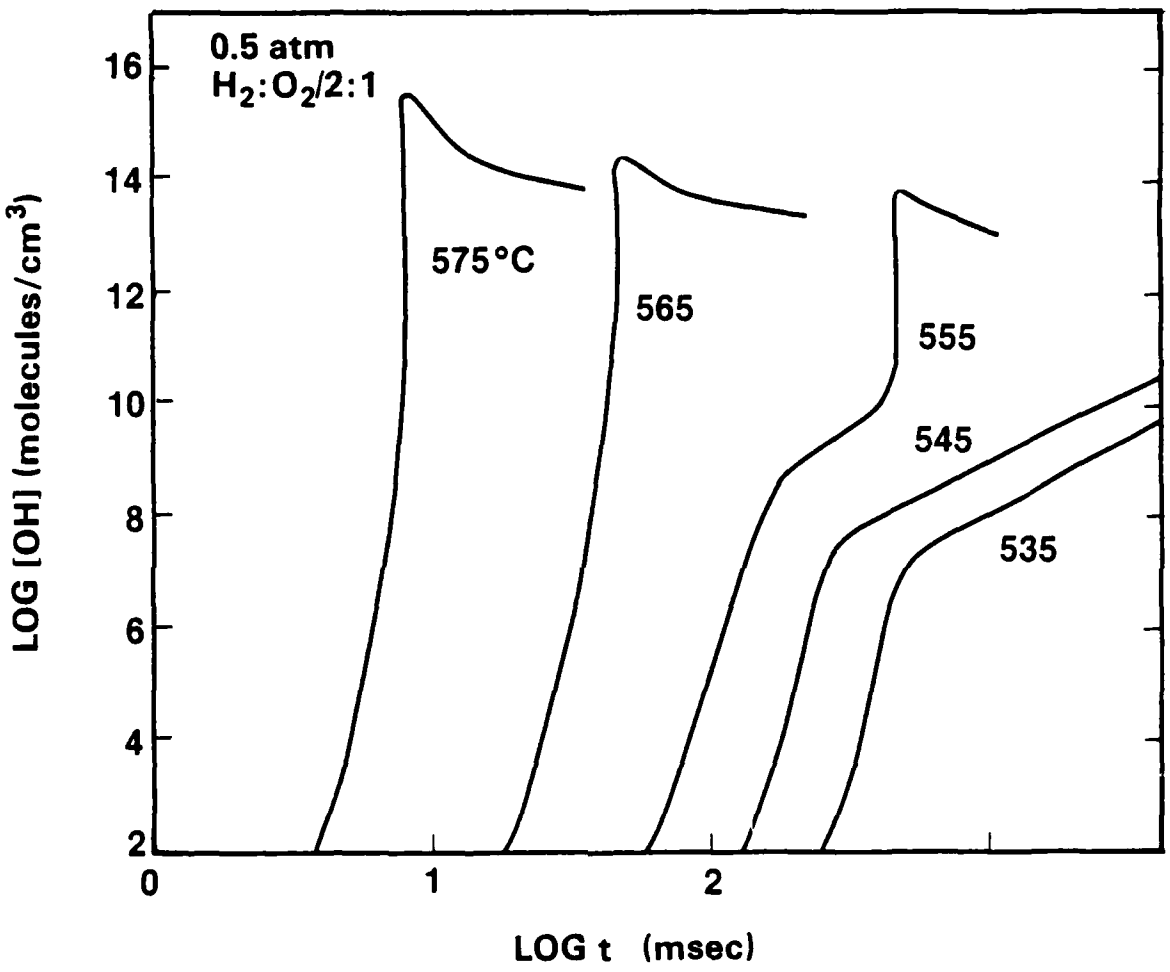

Fig. 16 — Temporal behavior of hydroxyl radical concentration, [HO], as a function of isothermal reaction temperature, T

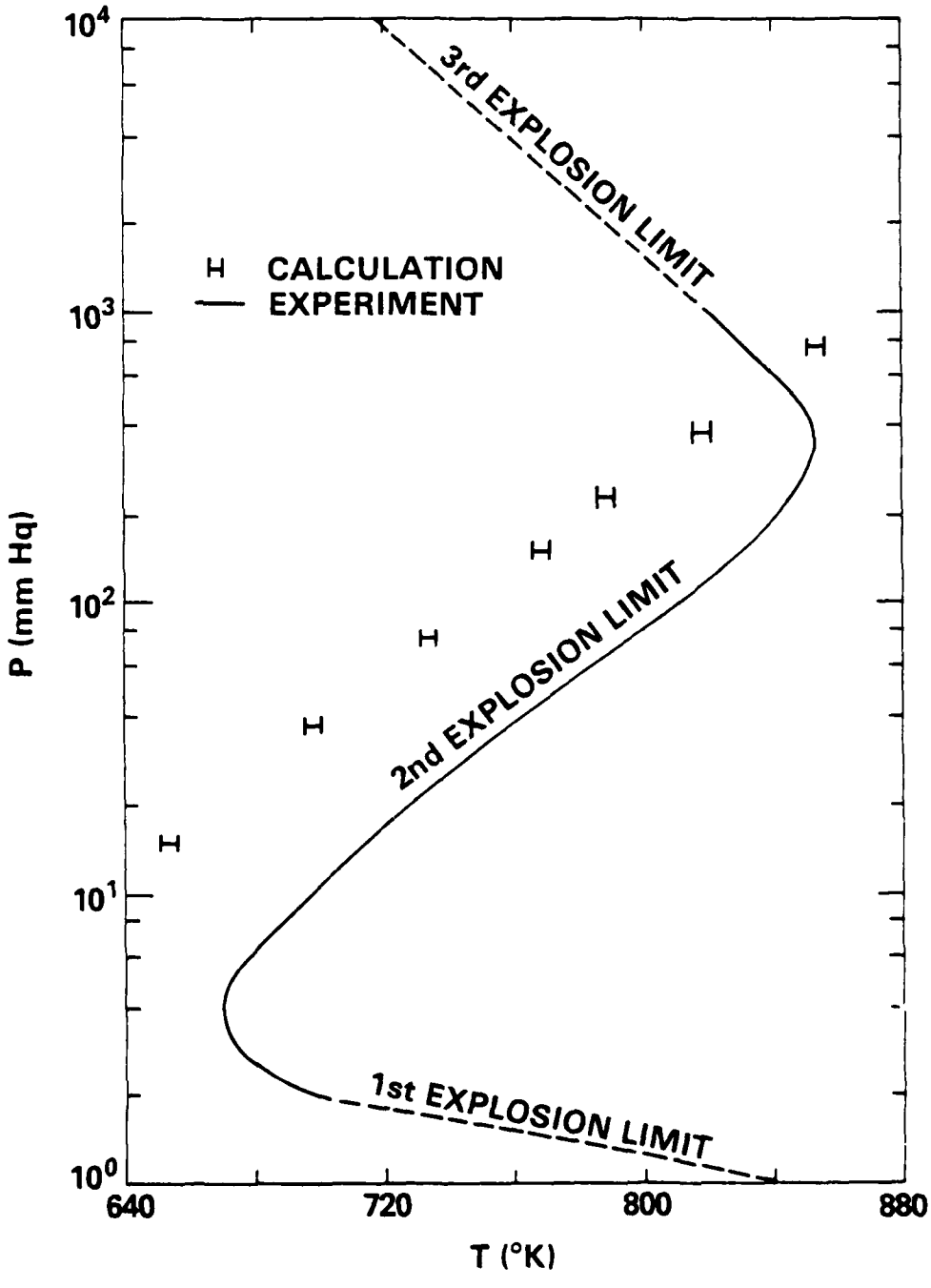

Fig. 17 — Comparison of computed and experimental explosion limits for H_2 O_2 2:1 gas mixtures. (The experimental data is taken from the work of Lewis and von Elbe [111].)

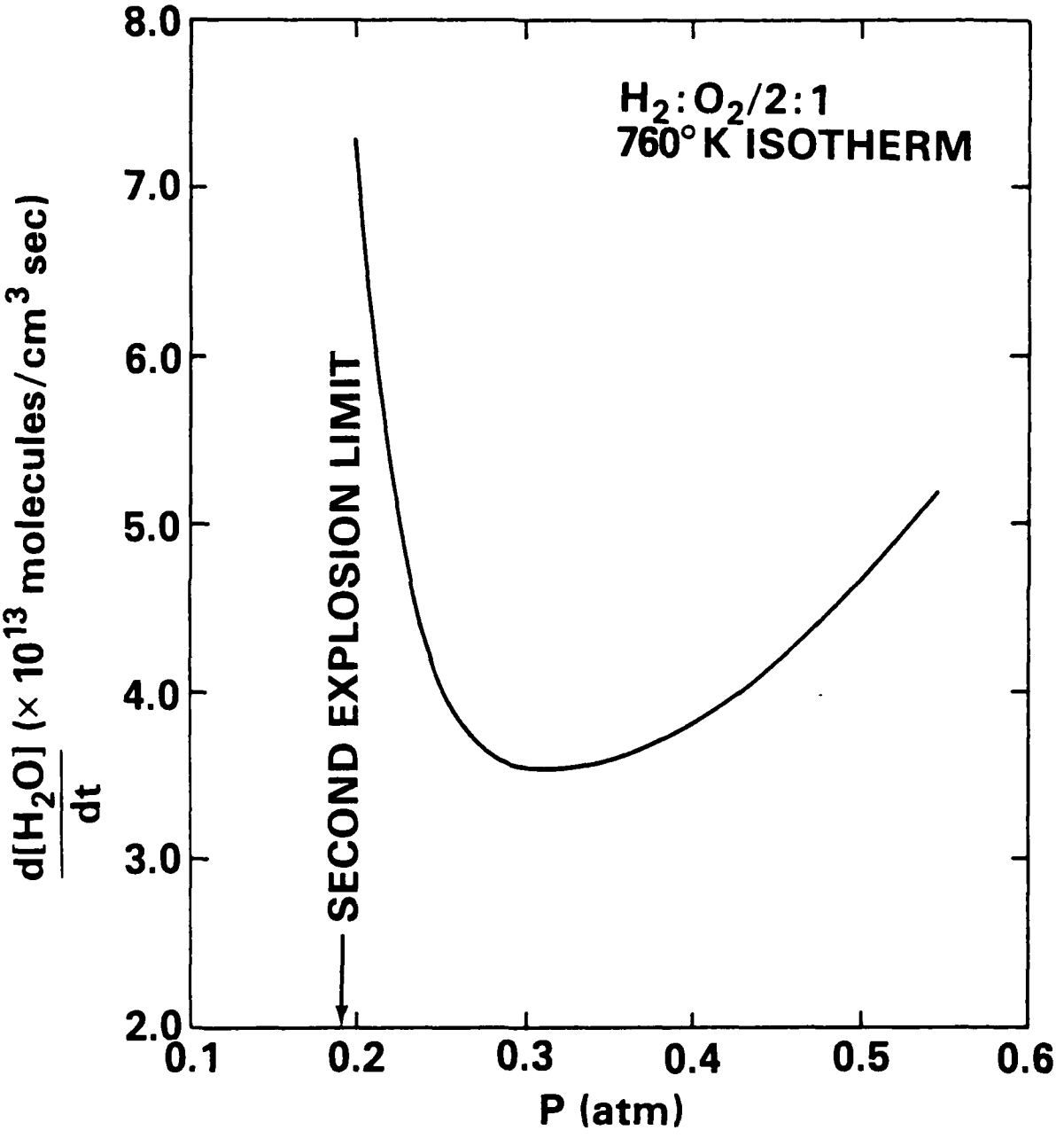

Fig. 18 — Computed isothermal plot of reaction rate, $\frac{d[H_2O]}{dt}$, as a function of pressure, P, above the 2nd explosion limit for a H_2:O_2 2:1 gas mixture

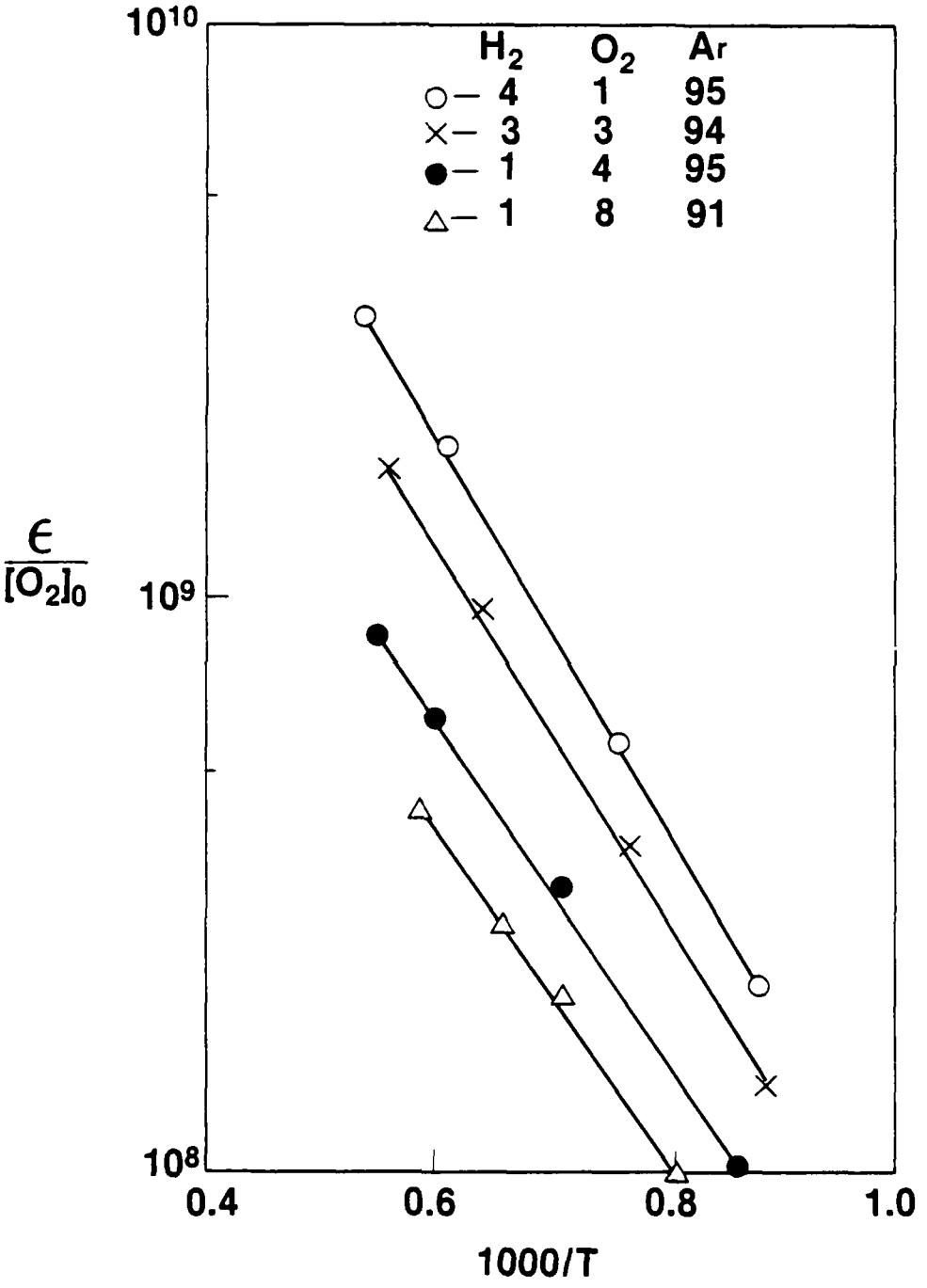

Fig. 19 — Exponential growth parameter to initial oxygen concentration ratio, $\epsilon/[O_2]_0$, as a function of 1000/T

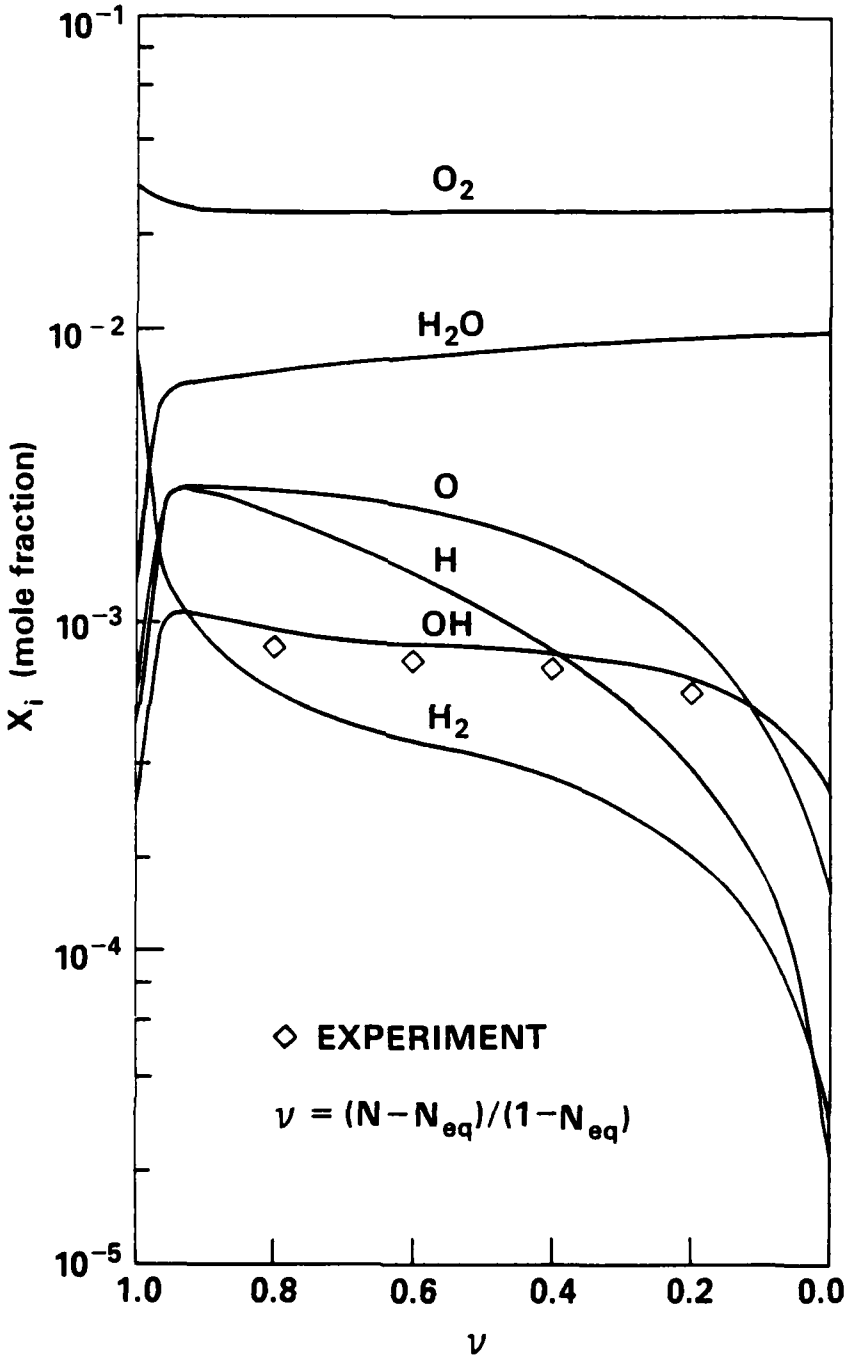

Fig. 20 — Comparison of computed and experimental temporal behavior of reaction species concentrations as a function of the reaction progress variable, ν

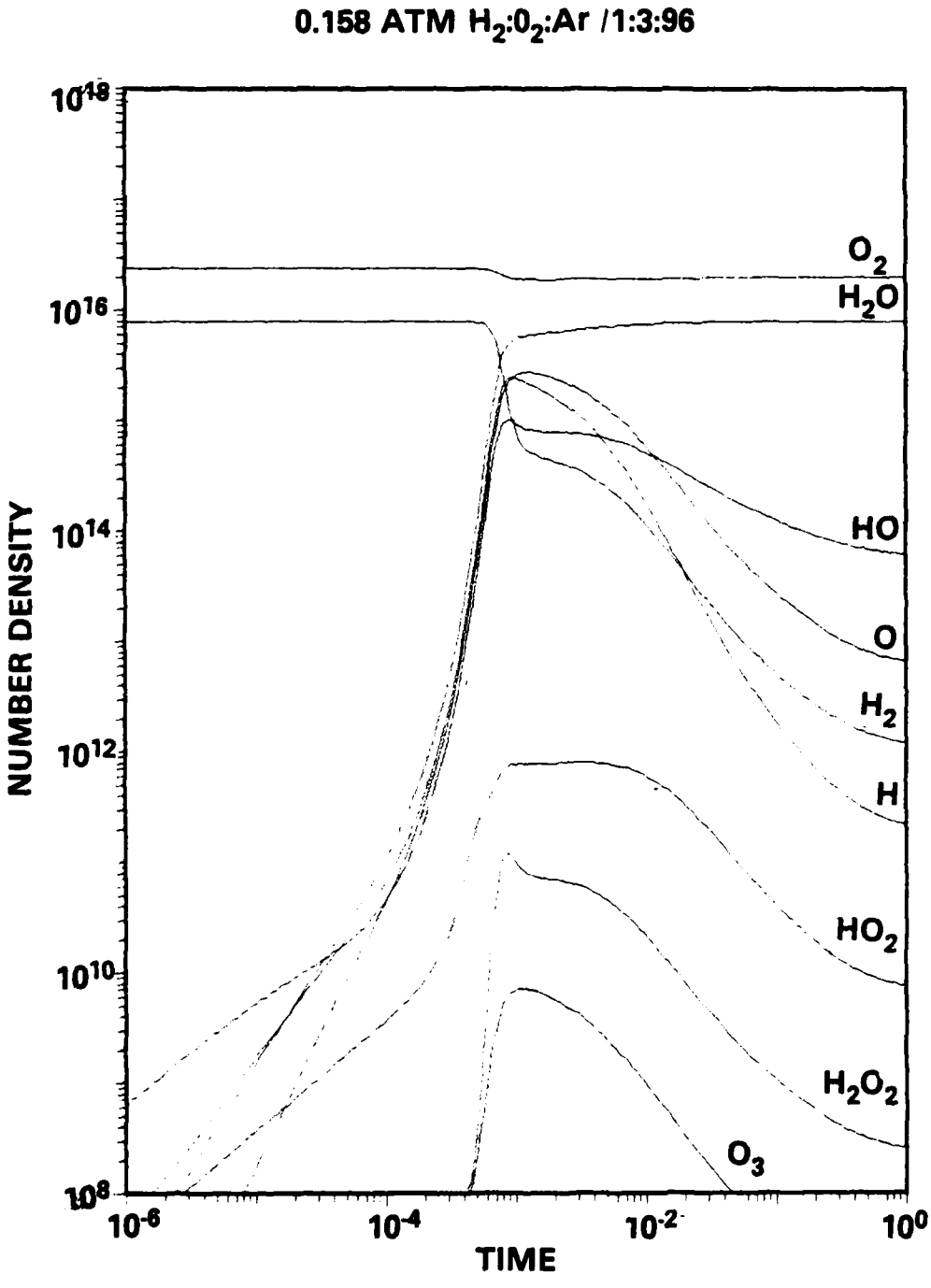

Fig. 21 – Computed temporal behavior of reaction species for a 0.158 atm of $H_2:O_2:Ar/1:3:96$

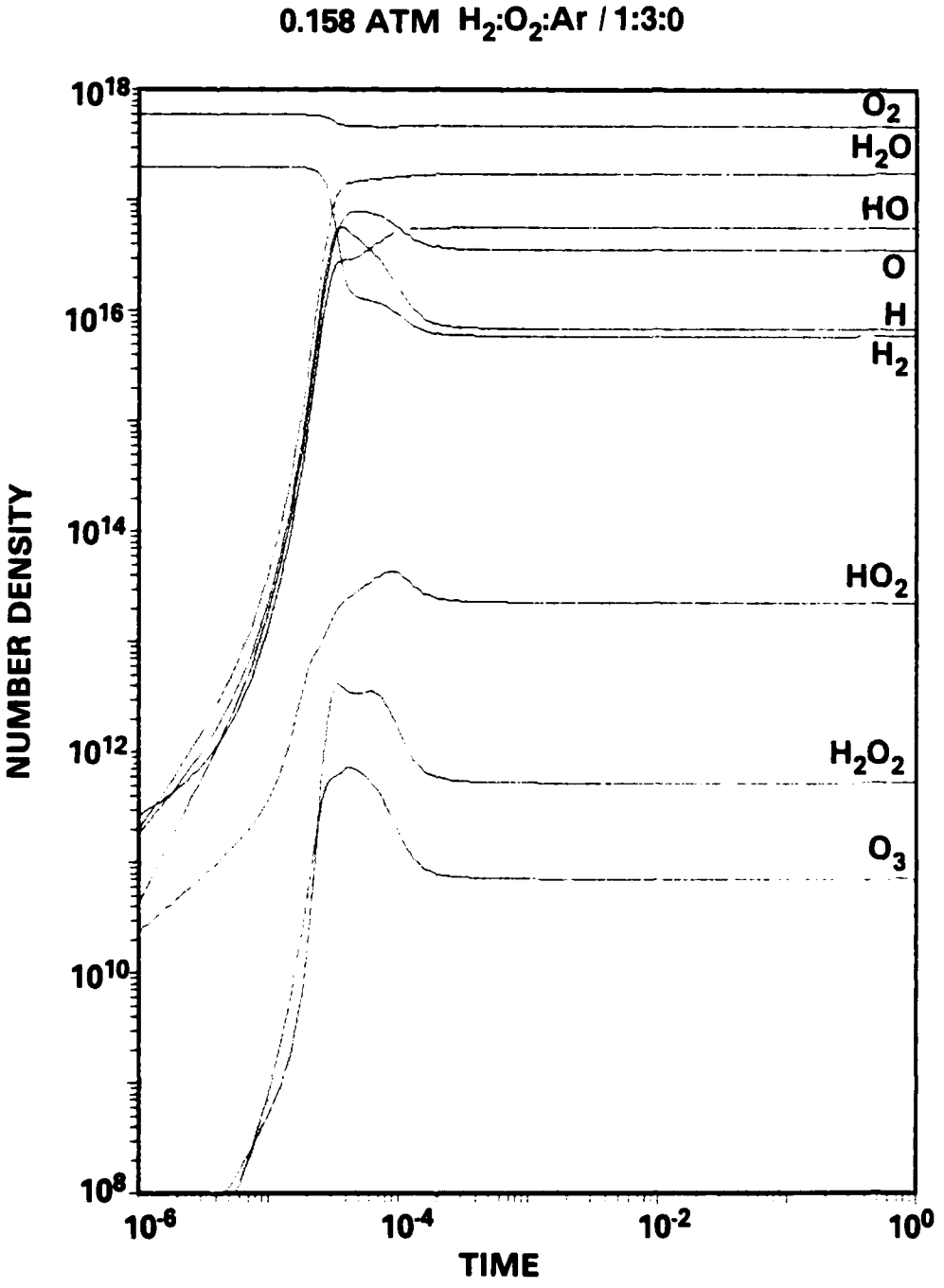

Fig. 22 — Computed temporal behavior of reaction species for a 0.158 atm of H_2:O_2:Ar/1:3:0